New General Relativity Tests

Alexander F. Zakharov

A. I. Alikhanov ITEP -- NRC "Kurchatov Institute"

BLTP, JINR, Dubna

The Scientific Coordination Session on "Non-Ideal Plasma Physics"
Joint Institute for High Temperatures, Moscow, Russia
7 December 2023

The first observation of black hole shadow in M87 using the Event Horizon Telescope

А.Ф. Захаров (Alexander F. Zakharov)

E-mail: zakharov@itep.ru

Institute of Theoretical and Experimental Physics,
B. Cheremushkinskaya, 25, 117218 Moscow

Bogoliubov Laboratory of Theoretical Physics
Joint Institute for Nuclear Research, Dubna, Russia

27.05.2019 Joint Institute for High Temperatures of the Russian Academy of Sciences, Moscow

Black hole types

- Black holes with stellar masses 10 -- 10^2 M_{Sun}
- Massive black holes 10^2 -- 10^5 M_{Sun}
- Supermassive black holes 10^5 – 10^{10} M_{sun}

How to probe a black hole

Albert Einstein's theory of gravity, general relativity, predicts that the collapse of enough mass can leave a self-sustaining gravitational field so strong that, inside a distance called the event horizon, nothing can escape, not even light. But are black holes exactly the inscrutable things general relativity predicts? Observers may now have the tools to find out.

1. Trace the stars

Tracking the orbits of stars around the black hole in our Galaxy's center can reveal whether the black hole warps space and time exactly as general relativity predicts.

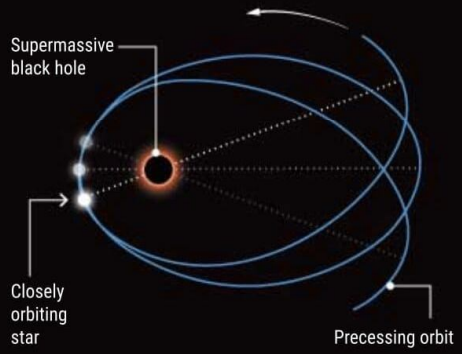

2. Take a picture

An image of a supermassive black hole holds clues to whether, as general relativity predicts, it has an event horizon rather than a surface, and mass and spin are its sole properties.

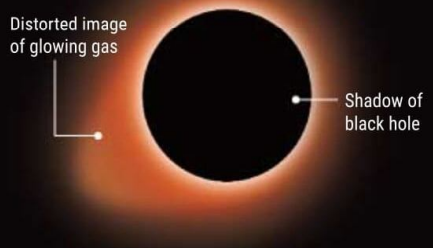

3. Catch the waves

When two small black holes spiral together, they radiate gravitational waves, which could reveal whether the supposed black holes are instead material objects. The final black hole reverberates at frequencies and overtones that provide another test of whether its only properties are mass and spin.

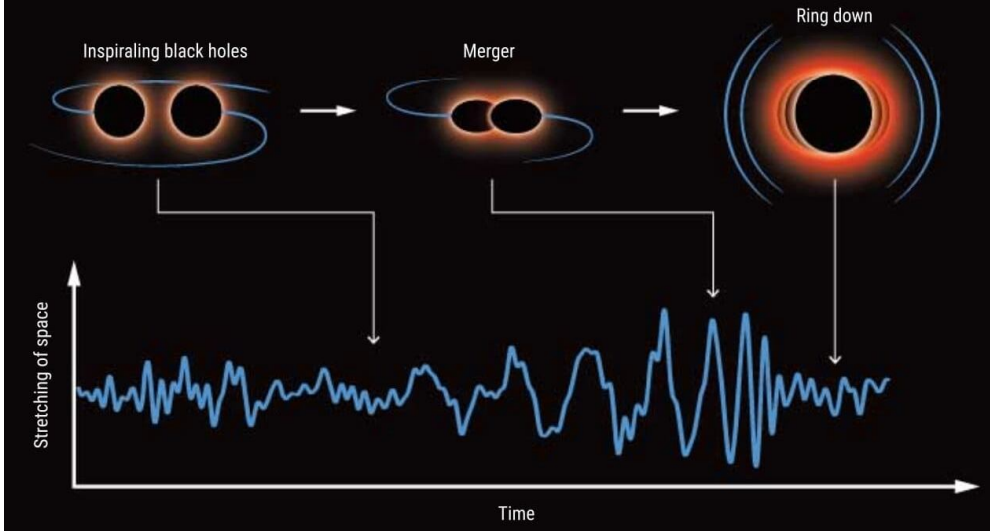

Great success of relativistic astrophysics

Three Nobel prizes in last five years (2017, 2019, 2020)

LIGO-Virgo: BBHs, BNS (kilonova) GW 170817;

GRAVITY, Keck and new tests of GR (gravitational redshift for S2 near its periapsis passage)

The confirmation of relativistic precession for S2 (GRAVITY)

Shadow reconstructions in M87* and Sgr A*

Coevolution (Or Not) of Supermassive Black Holes and Host Galaxies

John Kormendy[1] and Luis C. Ho[2]

[1]Department of Astronomy, University of Texas at Austin,
2515 Speedway C1400, Austin, TX 78712-1205; email: kormendy@astro.as.utexas.edu

[2]The Observatories of the Carnegie Institution for Science,
813 Santa Barbara Street, Pasadena, CA 91101; email: lho@obs.carnegiescience.edu

Abstract

Supermassive black holes (BHs) have been found in 87 galaxies by dynamical modeling of spatially resolved kinematics. The *Hubble Space Telescope* revolutionized BH research by advancing the subject from its proof-of-concept phase into quantitative studies of BH demographics. Most influential was the discovery of a tight correlation between BH mass $M_\bullet$ and the velocity dispersion σ of the bulge component of the host galaxy. Together with similar correlations with bulge luminosity and mass, this led to the widespread belief that BHs and bulges coevolve by regulating each other's growth. Conclusions based on one set of correlations from $M_\bullet \sim 10^{9.5}\ M_\odot$ in brightest cluster ellipticals to $M_\bullet \sim 10^6\ M_\odot$ in the smallest galaxies dominated BH work for more than a decade.

New results are now replacing this simple story with a richer and more plausible picture in which BHs correlate differently with different galaxy components. A reasonable aim is to use this progress to refine our understanding of BH – galaxy coevolution. BHs with masses of $10^5 - 10^6\ M_\odot$ are found in many bulgeless galaxies. Therefore, classical (elliptical-galaxy-like) bulges are not necessary for BH formation. On the other hand, while they live in galaxy disks, BHs do not correlate with galaxy disks. Also, any $M_\bullet$ correlations with the properties of disk-grown pseudobulges and dark matter halos are weak enough to imply no close coevolution.

The above and other correlations of host galaxy parameters with each other and with $M_\bullet$ suggest that there are four regimes of BH feedback. (1) Local, secular, episodic, and stochastic feeding of small BHs in largely bulgeless galaxies involves too little energy to result in coevolution. (2) Global feeding in major, wet galaxy mergers rapidly grows giant BHs in short-duration, quasar-like events whose energy feedback does affect galaxy evolution. The resulting hosts are classical bulges and coreless-rotating-disky ellipticals. (3) After these AGN phases and at the highest galaxy masses, maintenance-mode BH feedback into X-ray-emitting gas has the primarily negative effect of helping to keep baryons locked up in hot gas and thereby keeping galaxy formation from going to completion. This happens in giant, core-nonrotating-boxy ellipticals. Their properties, including their tight correlations between $M_\bullet$ and core parameters, support the conclusion that core ellipticals form by dissipationless major mergers. They inherit coevolution effects from smaller progenitor galaxies. Also, (4) independent of any feedback physics, in BH growth modes (2) and (3), the averaging that results from successive mergers plays a major role in decreasing the scatter in $M_\bullet$ correlations from the large values observed in bulgeless and pseudobulge galaxies to the small values observed in giant elliptical galaxies.

Table 1 Mass measurements of supermassive black holes in our Galaxy, M 31, and M 32

Galaxy	D (Mpc)	σ_e (km s^{-1})	$M_\bullet$ ($M_{\rm low}, M_{\rm high}$) ($M_\odot$)	$r_{\rm infl}$ (arcsec)	σ_* (arcsec)	$r_{\rm infl}/\sigma_*$	Reference
(1)	(2)	(3)	(4)	(5)	(6)	(7)	(8)
Galaxy			4.41(3.98–4.84) e6		0.0146	2868.	Meyer et al. 2012
Galaxy			4.2 (3.9 –4.6) e6		0.0139	3013.	Yelda et al. 2011
Galaxy	0.00828	105	4.30(3.94–4.66) e6	41.9	0.0146	2868.	Genzel, Eisenhauer & Gillessen 2010
Galaxy	0.00828	105	4.30(3.94–4.66) e6	41.9	0.0146	2868.	Gillessen et al. 2009a
Galaxy			4.09(3.74–4.43) e6		0.0148	2829.	Gillessen et al. 2009b
Galaxy			4.25(3.44–4.79) e6		0.0139	3013.	Ghez et al. 2008
Galaxy			3.80(3.60–4.00) e6		0.0056	7478.	Ghez et al. 2005
Galaxy			3.7 (3.3 –4.1) e6		0.0075	5583.	Ghez et al. 2003
Galaxy			3.8 (2.3 –5.4) e6		0.0155	2702.	Schödel et al. 2002
Galaxy			2.1 (1.3 –2.8) e6		0.113	371.	Chakrabarty & Saha 2001
Galaxy			3.1 (2.6 –3.6) e6		0.26	161.	Genzel et al. 2000
Galaxy			2.7 (2.5 –2.9) e6		0.39	107.	Ghez et al. 1998
Galaxy			2.70(2.31–3.09) e6		0.39	107.	Genzel et al. 1997
Galaxy			2.55(2.12–2.95) e6		0.39	107.	Eckart & Genzel 1997
Galaxy			2.8 (2.5 –3.1) e6		2.4	17.4	Genzel et al. 1996
Galaxy			2.0 (0.9 –2.9) e6		4.9	8.5	Haller et al. 1996
Galaxy			2.9 (2.0 –3.9) e6		3.4	12.3	Krabbe et al. 1995
Galaxy			2. e6		5	8.4	Evans & de Zeeuw 1994
Galaxy			3. e6		5	8.4	Kent 1992
Galaxy			5.4 (3.9 –6.8) e6		15	2.8	Sellgren et al. 1990
M 31	0.774	169	1.4 (1.1–2.3) e8	5.75	0.053	109.	Bender et al. 2005
M 31			1.0 e8		0.297	19.4	Peiris & Tremaine 2003
M 31			6.1 (3.6–8.7) e7		0.052	111.	Bacon et al. 2001
M 31			3.3 (1.5–4.5) e7		0.297	19.4	Kormendy & Bender 1999
M 31			6.0 (5.8–6.2) e7		0.297	19.4	Magorrian et al. 1998
M 31			9.5 (7 – 10) e7		0.42	13.7	Emsellem & Combes 1997
M 31			7.5 e7		0.56	10.3	Tremaine 1995
M 31			8.0 e7		0.42	13.7	Bacon et al. 1994
M 31			5 (4.5–5.6) e7		0.59	9.7	Richstone, Bower & Dressler 1990
M 31			3.8 (1.1– 11) e7		0.56	10.3	Kormendy 1988a
M 31			5.6 (3.4–7.8) e7		0.59	9.7	Dressler & Richstone 1988
M 32	0.805	77	2.45(1.4–3.5) e6	0.46	0.052	8.76	van den Bosch & de Zeeuw 2010
M 32			2.9 (2.7–3.1) e6		0.052	8.76	Verolme et al. 2002
M 32			3.5 (2.3–4.6) e6		0.052	8.76	Joseph et al. 2001
M 32			2.4 (2.2–2.6) e6		0.23	1.98	Magorrian et al. 1998
M 32			3.9 (3.1–4.7) e6		0.050	9.11	van der Marel et al. 1998a
M 32			3.9 (3.3–4.5) e6		0.050	9.11	van der Marel et al. 1997a, 1997b
M 32			3.2 (2.6–3.7) e6		0.23	1.98	Bender, Kormendy & Dehnen 1996
M 32			2.1 (1.8–2.3) e6		0.34	1.34	Dehnen 1995
M 32			2.1 e6		0.34	1.34	Qian et al. 1995
M 32			2.1 (1.7–2.4) e6		0.34	1.34	van der Marel et al. 1994a
M 32			2.2 (0.8–3.5) e6		0.59	0.77	Richstone, Bower & Dressler 1990
M 32			9.3 e6		0.59	0.77	Dressler & Richstone 1988
M 32			7.5 (3.5–11.5) e6		0.76	0.60	Tonry 1987
M 32			5.8 e6		1.49	0.31	Tonry 1984

Lines based on HST spectroscopy are in red. Column 2 is the assumed distance. Column 3 is the stellar velocity dispersion inside the "effective radius" that encompasses half of the light of the bulge. Column 4 is the measured BH mass with the one-sigma range that includes 68 % of the probability in parentheses. Only the top four $M_\bullet$ values for the Galaxy include distance uncertainties in the error bars. Column 5 is the radius of the sphere of influence of the BH; the line that lists $r_{\rm infl}$ contains the adopted $M_\bullet$. Column 6 is the effective resolution of the spectroscopy, estimated as in Kormendy (2004). It is a radius that measures the blurring effects of the telescope point-spread function or "PSF," the slit width or aperture size, and the pixel size. The contribution of the telescope is estimated by the dispersion $\sigma_{*\rm tel}$ of a Gaussian fitted to the core of the average radial brightness profile of the PSF. In particular, the HST PSF has $\sigma_{*\rm tel} \simeq 0''.036$ from a single-Gaussian fit to the PSF model in van der Marel, de Zeeuw & Rix (1997a).

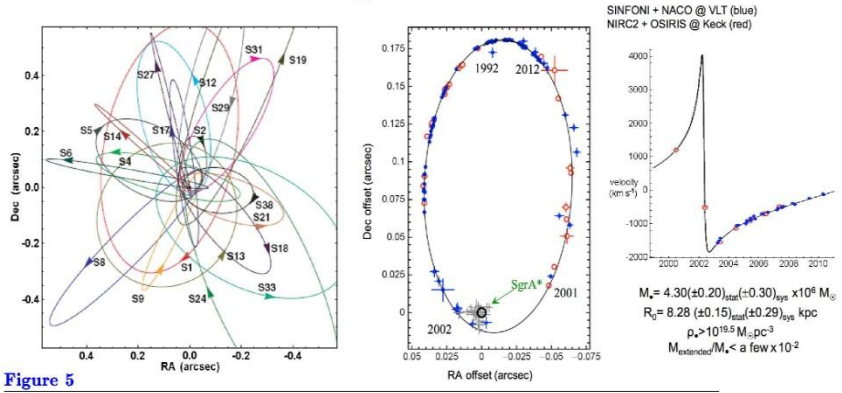

Figure 5

(*left*) Orbits of individual stars near the Galactic center. (*right*) Orbit of star S2 around the BH and associated radio source Sgr A* based on observations of its position from 1992 to 2012. Results from the Ghez group using the Keck telescope and from the Genzel group using the Europen Very Large Telescope (VLT) are combined. This figure is updated from Genzel, Eisenhauer & Gillessen (2010) and is kindly provided by Reinhard Genzel.

These results establish the existence and mass of the central dark object beyond any reasonable doubt. They also eliminate astrophysical plausible alternatives to a BH. These include brown dwarfs and stellar remnants (e. g., Maoz 1995, 1998; Genzel et al. 1997, 2000; Ghez et al. 1998, 2005) and even fermion balls (Ghez et al. 2005; GEG10). Boson balls (Torres et al. 2000; Schunck & Mielke 2003; Liebling & Palenzuela 2012) are harder to exclude; they are highly relativistic, they do not have hard surfaces, and they are consistent with dynamical mass and size constraints. But a boson ball is like the proverbial elephant in a tree: it is OK where it is, but how did it ever get there? GEG10 argue that boson balls are inconsistent with astrophysical constraints based on AGN radiation. Also, the Sołtan (1982) argument implies that at least most of the central dark mass observed in galaxies grew by accretion in AGN phases, and this quickly makes highly relativistic objects collapse into BHs. Finally (Fabian 2013), X-ray AGN observations imply that we see, in some objects, material interior to the innermost stable circular orbit of a non-rotating BH; this implies that these BHs are rotating rapidly and excludes boson balls as alternatives to all central dark objects. Arguments against the most plausible BH alternatives – failed stars and dead stars – are also made for other galaxies in Maoz (1995, 1998) and in Bender et al. (2005). Exotica such as sterile neutrinos or dark matter WIMPs could still have detectable (small) effects, but we conclude that they no longer threaten the conclusion that we are detecting supermassive black holes.

KR95 was titled "Inward Bound – The Search for Supermassive Black Holes in Galactic Nuclei." HST has taken us essentially one order of magnitude inward in radius. A few other telescopes take us closer. But mostly, we are still working at 10^4 to 10^5 Schwarzschild radii. In our Galaxy, we have observed individual stars in to $\sim$ 500 Schwarzschild radii. Only the velocity profiles of relativistically broadened Fe Kα lines (e. g., Tanaka et al. 1995; Fabian 2013) probe radii that are comparable to the Schwarzschild radius. So we are still inward bound. Joining up our measurements made at thousands of r_S with those probed by Fe Kα emission requires that we robustly integrate into our story the rich and complicated details of AGN physics; that is, the narrow– and broad–emission-line regions. That journey still has far to go.

Massive graviton theories

- M. Fierz and W.Pauli-1939
- Zakharov; Veltman, van Dam – 1970
- Vainshtein - 1972
- Boulware, Deser -- 1972
- Logunov, Mestvirishvili, Gershtein et al. (RTG)
- Visser – 1998 (review on such theories)
- Rubakov, Tinyakov – 2008
- de Rham et al.—2011 -- 2016

Journal of Cosmology and Astroparticle Physics
An IOP and SISSA journal

Constraining the range of Yukawa gravity interaction from S2 star orbits II: bounds on graviton mass

A.F. Zakharov,[a,b,c,d,e] **P. Jovanović,**[f] **D. Borka**[g] **and V. Borka Jovanović**[g]

[a]National Astronomical Observatories of Chinese Academy of Sciences, Datun Road 20A, Beijing, 100012 China
[b]Institute of Theoretical and Experimental Physics, 117259 Moscow, Russia
[c]National Research Nuclear University MEPhI (Moscow Engineering Physics Institute), 115409, Moscow, Russia
[d]Bogoliubov Laboratory for Theoretical Physics, JINR, 141980 Dubna, Russia
[e]North Carolina Central University, Durham, NC 27707, U.S.A.
[f]Astronomical Observatory, Volgina 7, 11060 Belgrade, Serbia
[g]Atomic Physics Laboratory (040), Vinča Institute of Nuclear Sciences, University of Belgrade, P.O. Box 522, 11001 Belgrade, Serbia

E-mail: zakharov@itep.ru, pjovanovic@aob.rs, dusborka@vin.bg.ac.rs, vborka@vin.bg.ac.rs

Received May 4, 2016
Accepted May 7, 2016
Published May 20, 2016

Abstract. Recently LIGO collaboration discovered gravitational waves [1] predicted 100 years ago by A. Einstein. Moreover, in the key paper reporting about the discovery, the joint LIGO & VIRGO team presented an upper limit on graviton mass such as $m_g < 1.2 \times 10^{-22} eV$ [1] (see also more details in another LIGO paper [2] dedicated to a data analysis to obtain such a small constraint on a graviton mass). Since the graviton mass limit is so small the authors concluded that their observational data do not show violations of classical general relativity. We consider another opportunity to evaluate a graviton mass from phenomenological consequences of massive gravity and show that an analysis of bright star trajectories could bound graviton mass with a comparable accuracy with accuracies reached with gravitational wave interferometers and expected with forthcoming pulsar timing observations for gravitational wave detection. It gives an opportunity to treat observations of

JCAP05(2016)045

doi:10.1088/1475-7516/2016/05/045

Constraints on graviton mass from S2 trajectory

- AFZ, D. Borka, P. Jovanovic, V. Borka Jovanovic gr-qc: 1605.00913v; JCAP (2016) :
- $\lambda_g > 2900$ AU = 4.3×10^{11} km with P=0.9 or
- $m_g < 2.9 \times 10^{-21}$ eV $= 5.17 \times 10^{-54}$ g
- Hees et al. PRL (2017) slightly improved our estimates with their new data $m_g < 1.6 \times 10^{-21}$ eV (see discussion below)

graviton MASS

INSPIRE search

It is likely that the graviton is massless. More than fifty years ago Van Dam and Veltman (VANDAM 1970), Iwasaki (IWASAKI 1970), and Zakharov (ZAKHAROV 1970) almost simultaneously showed that in the linear approximation a theory with a finite graviton mass does not approach GR as the mass approaches zero. Attempts have been made to evade this "vDVZ discontinuity" by invoking modified gravity or nonlinear theory by De Rahm (DE-RHAM 2017) and others. More recently, the analysis of gravitational wave dispersion has led to bounds that are largely independent of the underlying model, even if not the strongest. We quote the best of these as our best limit.

Experimental limits have been set based on a Yukawa potential (YUKA), dispersion relation (DISP), or other modified gravity theories (MGRV).

The following conversions are useful: 1 eV = 1.783×10^{-33} g = $1.957 \times 10^{-6} m_e$; $\lambda_C = (1.973 \times 10^{-7}\ \text{m}) \times (1\ \text{eV}/m_g)$.

VALUE (eV)	*DOCUMENT ID*		*TECN*	*COMMENT*
$< 5 \times 10^{-23}$	[1] ABBOTT	2019	DISP	LIGO Virgo catalog GWTC-1
• • We do not use the following data for averages, fits, limits, etc. • •				
$< 3.2 \times 10^{-23}$	[2] BERNUS	2020	YUKA	Planetary ephemeris INPOP19a
$< 2 \times 10^{-28}$	[3] SHAO	2020	DISP	Binary pulsar Galileon radiation
$< 7 \times 10^{-23}$	[4] BERNUS	2019	YUKA	Planetary ephemeris INPOP17b
$< 3.1 \times 10^{-20}$	[5] MIAO	2019	DISP	Binary pulsar orbital decay rate
$< 1.4 \times 10^{-29}$	[6] DESAI	2018	YUKA	Gal cluster Abell 1689
$< 5 \times 10^{-30}$	[7] GUPTA	2018	YUKA	Using SPT-SZ
$< 3 \times 10^{-30}$	[7] GUPTA	2018	YUKA	Using Planck all-sky SZ
$< 1.3 \times 10^{-29}$	[7] GUPTA	2018	YUKA	Using redMaPPer SDSS-DR8
$< 6 \times 10^{-30}$	[8] RANA	2018	YUKA	Weak lensing in massive clusters
$< 8 \times 10^{-30}$	[9] RANA	2018	YUKA	SZ effect in massive clusters
$< 1.0 \times 10^{-23}$	[10] WILL	2018	YUKA	Perihelion advances of planets
$< 7 \times 10^{-23}$	[1] ABBOTT	2017	DISP	Combined dispersion limit from three BH mergers
$< 1.2 \times 10^{-22}$	[1] ABBOTT	2016	DISP	Combined dispersion limit from two BH mergers
$< 2.9 \times 10^{-21}$	[11] ZAKHAROV	2016	YUKA	S2 star orbit
$< 5 \times 10^{-23}$	[12] BRITO	2013	MGRV	Spinning black holes bounds
$< 6 \times 10^{-32}$	[13] GRUZINOV	2005	MGRV	Solar System observations
$< 6 \times 10^{-32}$	[14] CHOUDHURY	2004	YUKA	Weak gravitational lensing
$< 9.0 \times 10^{-34}$	[15] GERSHTEIN	2004	MGRV	From Ω_{tot} value assuming RTG
$< 8 \times 10^{-20}$	[16, 17] FINN	2002	DISP	Binary pulsar orbital period decrease
$< 7 \times 10^{-23}$	TALMADGE	1988	YUKA	Solar system planetary astrometric data
$< 1.3 \times 10^{-29}$	[18] GOLDHABER	1974	YUKA	Rich clusters
$< 7 \times 10^{-28}$	HARE	1973	YUKA	Galaxy
$< 8 \times 10^{4}$	HARE	1973	YUKA	2γ decay

[1] ABBOTT 2019 , ABBOTT 2017 , and ABBOTT 2016 limits assume a dispersion relation for gravitational waves modified relative to GR.

[2] BERNUS 2020 use the latest solution of the ephemeris INPOP (19a) in order to improve the constraint in BERNUS 2019 on the existence of a Yukawa suppression to the Newtonian potential, generically associated to a gravitons mass.

[3] SHAO 2020 sets limit, 95% CL, based on non-observation of excess gravitational radiation in 14 well-timed binary pulsars in the context of the cubic Galileon model.

[4] BERNUS 2019 use the planetary ephemeris INPOP 17b to constraint the existence of a Yukawa suppression to the Newtonian potential, generically associated to a gravitons mass.

[5] MIAO 2019 90% CL limit is based on orbital period decay rates of 9 binary pulsars using a Bayesian prior uniform in graviton mass. Limit becomes $< 5.2 \times 10^{-21}$ eV for a prior uniform in $\ln(m_g)$.

[6] DESAI 2018 limit based on dynamical mass models of galaxy cluster Abell 1689.

VALUE (eV)	*DOCUMENT ID*	*TECN*	*COMMENT*

[7] GUPTA 2018 obtains graviton mass limits using stacked clusters from 3 disparate surveys.

[8] RANA 2018 limit, 68% CL, obtained using weak lensing mass profiles out to the radius at which the cluster density falls to 200 times the critical density of the Universe. Limit is based on the fractional change between Newtonian and Yukawa accelerations for the 50 most massive galaxy clusters in the Local Cluster Substructure Survey. Limits for other CL's and other density cuts are also given.

[9] RANA 2018 limit, 68% CL, obtained using mass measurements via the SZ effect out to the radius at which the cluster density falls to 500 times the critical density of the Universe for 182 optically confirmed galaxy clusters in an Altacama Cosmology Telescope survey. Limits for other CL's and other density cuts are also given.

[10] WILL 2018 limit from perihelion advances of the planets, notably Earth, Mars, and Saturn. Alternate analysis yields $< 6 \times 10^{-24}$.

[11] ZAKHAROV 2016 constrains range of Yukawa gravity interaction from S2 star orbit about black hole at Galactic center. The limit is $< 2.9 \times 10^{-21}$ eV for $\delta = 100$.

[12] BRITO 2013 explore massive graviton (spin-2) fluctuations around rotating black holes.

[13] GRUZINOV 2005 uses the DGP model (DVALI 2000) showing that non-perturbative effects restore continuity with Einstein's equations as the gravition mass approaches zero, then bases his limit on Solar System observations.

[14] CHOUDHURY 2004 concludes from a study of weak-lensing data that masses heavier than about the inverse of 100 Mpc seem to be ruled out if the gravitation field has the Yukawa form.

[15] GERSHTEIN 2004 use non-Einstein field relativistic theory of gravity (RTG), with a massive graviton, to obtain the 95% CL mass limit implied by the value of Ω_{tot} = 1.02 ± 0.02 current at the time of publication.

[16] FINN 2002 analyze the orbital decay rates of PSR B1913+16 and PSR B1534+12 with a possible graviton mass as a parameter. The combined frequentist mass limit is at 90%CL.

[17] As of 2020, limits on dP/dt are now about 0.1% (see T. Damour, "Experimental tests of gravitational theory," in this *Review*).

[18] GOLDHABER 1974 establish this limit considering the binding of galactic clusters, corrected to Planck h_0 = 0.67.

References:

BERNUS	2020	PR D102 021501	Constraint on the Yukawa suppression of the Newtonian potential from the planetary ephemeris INPOP19a
SHAO	2020	PR D102 024069	New Graviton Mass Bound from Binary Pulsars
ABBOTT	2019	PR D100 104036	Tests of General Relativity with the Binary Black Hole Signals from the LIGO-Virgo Catalog GWTC-1
BERNUS	2019	PRL 123 161103	Constraining the mass of the graviton with the planetary ephemeris INPOP
MIAO	2019	PR D99 123015	Bounding the mass of graviton in a dynamic regime with binary pulsars
DESAI	2018	PL B778 325	Limit on graviton mass from galaxy cluster Abell 1689
GUPTA	2018	ANP 399 85	Limit on graviton mass using stacked galaxy cluster catalogs from SPT-SZ, Planck-SZ and SDSS-redMaPPer
RANA	2018	PL B781 220	Bounds on graviton mass using weak lensing and SZ effect in galaxy clusters
WILL	2018	CQG 35 17LT01	Solar system versus gravitational-wave bounds on the graviton mass
ABBOTT	2017	PRL 118 221101	GW170104: Observation of a 50-Solar-Mass Binary Black Hole Coalescence at Redshift 0.2
ABBOTT	2016	PRL 116 061102	Observation of Gravitational Waves from a Binary Black Hole Merger
ZAKHAROV	2016	JCAP 1605 045	Constraining the range of Yukawa gravity interaction from S2 star orbits II: Bounds on graviton mass
BRITO	2013	PR D88 023514	Massive Spin-2 Fields on Black Hole Spacetimes: Instability of the Schwarzschild and Kerr Solutions and Bounds on the Graviton Mass
GRUZINOV	2005	NAST 10 311	On the Graviton Mass
CHOUDHURY	2004	ASP 21 559	Probing Large Distance Higher Dimensional Gravity from Lensing Data
GERSHTEIN	2004	PAN 67 1596	Graviton Mass, Quintessence and Oscillatory Character of the Universe Evolution
FINN	2002	PR D65 044022	Bounding the Mass of the Graviton using Binary Pulsar Observations
TALMADGE	1988	PRL 61 1159	Model Independent Constraints on Possible Modifications of Newtonian Gravity
GOLDHABER	1974	PR D9 1119	Mass of the Graviton
HARE	1973	CJP 51 431	Mass of the Graviton

Shadow reconstructions for M87* and Sgr A* are based on three pillars: Synchrotron radiation, VLBI concept, GR in a strong gravitational field

Synchrotron radiation George A. Schott)

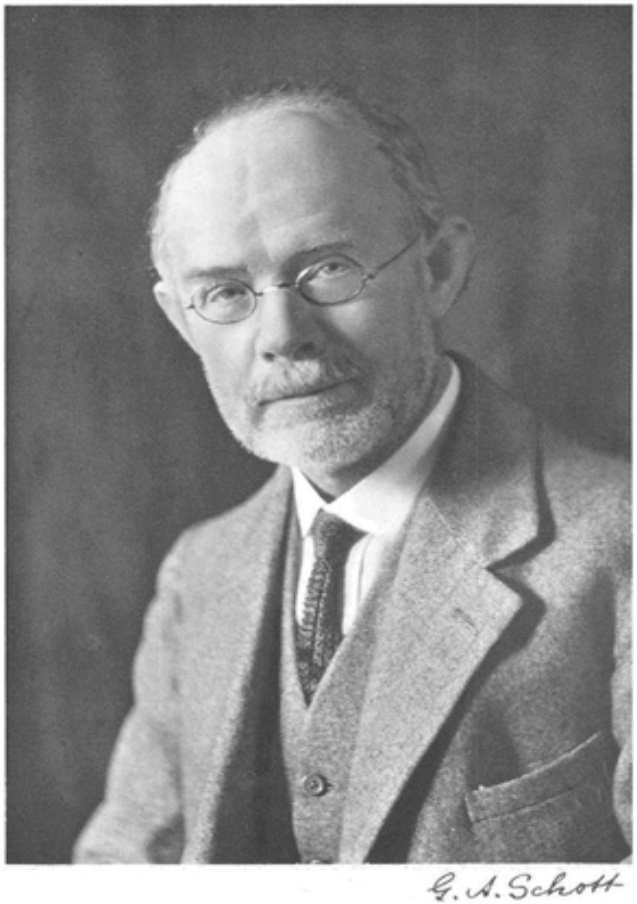

ELECTROMAGNETIC RADIATION

AND THE MECHANICAL REACTIONS ARISING FROM IT

BEING AN ADAMS PRIZE ESSAY IN THE UNIVERSITY OF CAMBRIDGE

by

G. A. SCHOTT, B.A., D.Sc.

Professor of Applied Mathematics in the University College of Wales, Aberystwyth
Formerly Scholar of Trinity College, Cambridge

Cambridge:
at the University Press
1912

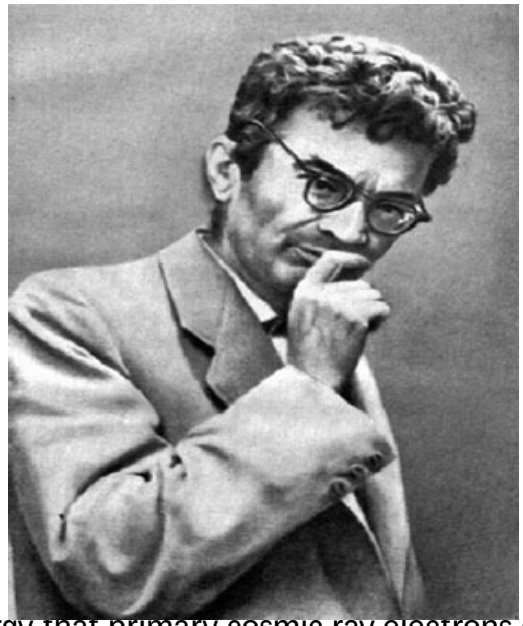

I. Pomeranchuk, The maximum energy that primary cosmic ray electrons can have on the Earth's surface due to radiation in the Earth's magnetic field, J. Phys. USSR, 2, 356 (1940)

D. Ivanenko and I. Pomeranchuk, On the Maximal Energy Attainable in a Betatron, Phys. Rev. 65, 343 (1944)

L.A. Artsimovich and I. Pomeranchuk, The maximum energy that primary cosmic ray electrons can have on the Earth's surface due to radiation in the Earth's magnetic field, J. Phys. USSR, 2, 267 (1945)

Elder, F. R., Gurewitsch, A. M., Langmuir, R. V., & Pollock, H. C. Radiation from Electrons in a Synchrotron. Physical Review, 71(11), 829 (1947)

In 1950 D. Ivanenko, A. A. Sokolov and I. Pomeranchuk were awarded the State prize of the second grade for works on synchrotron radiation, presented in book “Classical Field Theory”

Synchrotron radiation plays a key role in many astrophysical objects (including BH's and pulsars (Crab Nebula)) . In 1946 they predicted emission in radio band from solar corona. In May 1947 they participated in Brazil expedition

The Soviet expedition in Brazil for solar eclipse observations in 20 May 1947 where S. E. Khaikin and B. M. Chikhachev discovered radio emission from solar corona during the solar eclipse aboard the “Griboedov” ship

The idea of VLBI observation was introduced by L. I. Matveenko (1929—2019) in 1960s and it was realized in Soviet – US joint radio observations in 1970s. Matveenko proposed also a project of a ground – space interferometer. This idea was realized later by Japanese (HALCA, VSOP, 1997) and Russian Astronomers (Radioastron, 2011) .

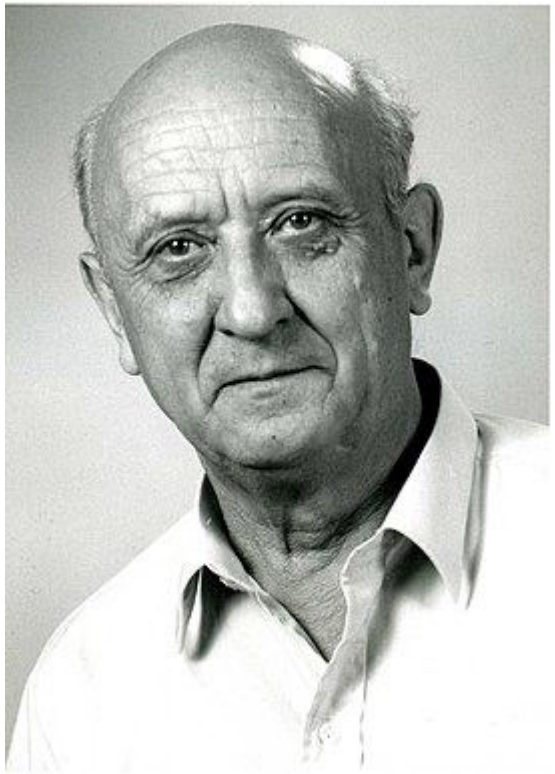

EHT shadow reconstruction for M87* and Sgr A* observed in April 2017

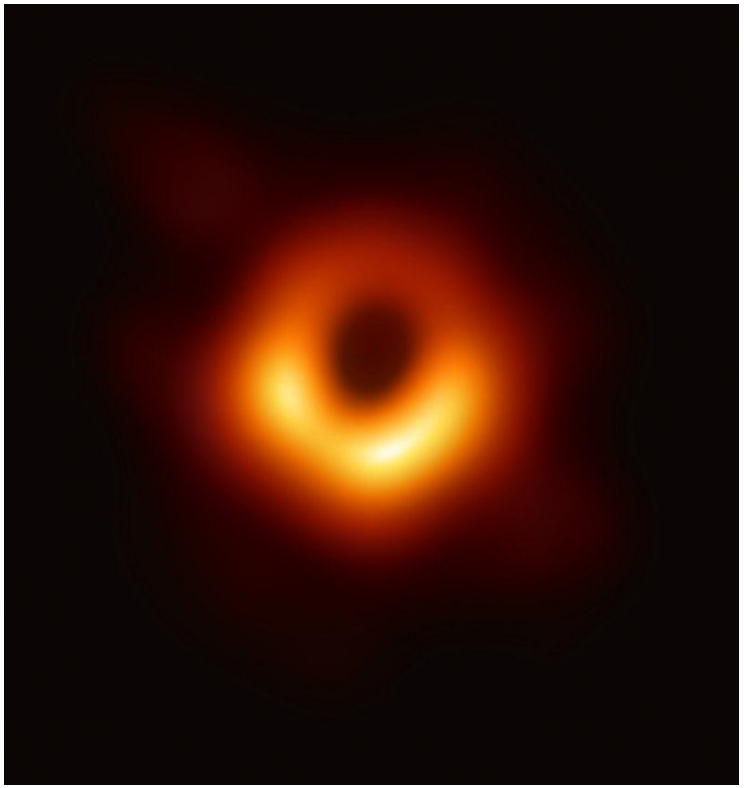

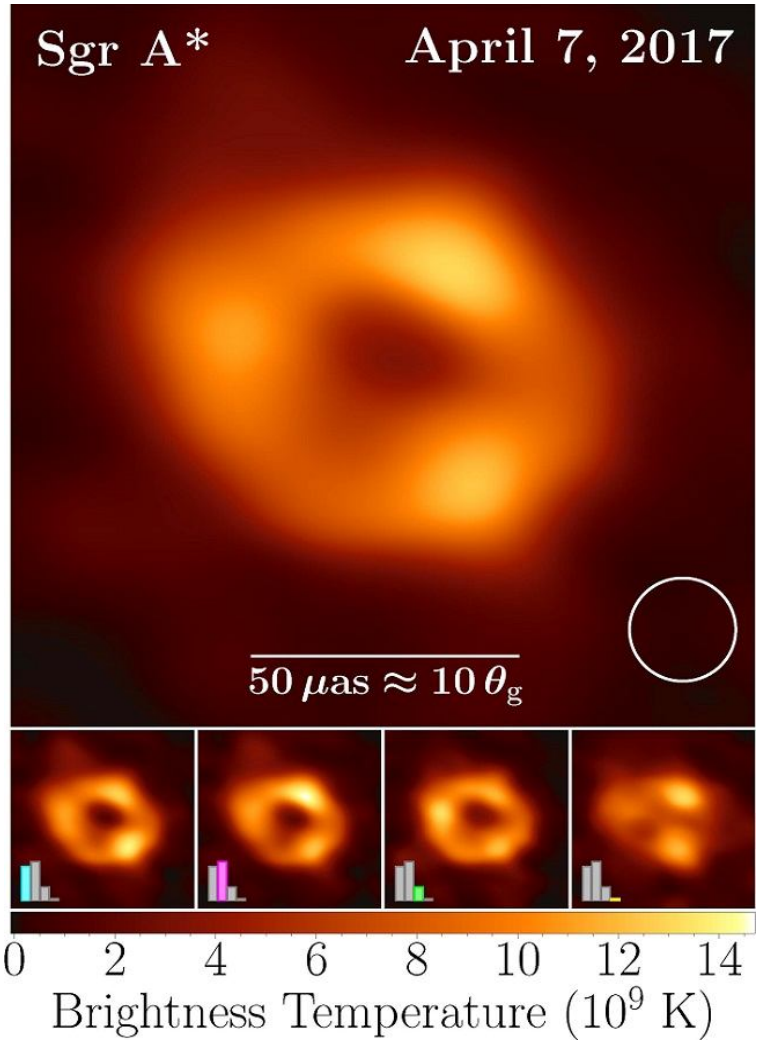

Подтверждено предсказание ученого НИЦ "Курчатовский институт" о существовании "тени" в центре нашей Галактики

15.06.2022 ПРЕСС-ЦЕНТР НИЦ "КУРЧАТОВСКИЙ ИНСТИТУТ"

Фото: Ana Torres Kampos

В 2005 году физик-теоретик **Александр Захаров** и его соавторы предложили с помощью наблюдений подтвердить присутствие сверхмассивной черной дыры в Центре нашей Галактики и проверить предсказания общей теории относительности в сильном гравитационном поле. А. Захаров и его итальянские коллеги предположили, что в случае наличия черной дыры в Галактическом центре (ГЦ) наблюдатели в направлении на ГЦ увидят тень размером порядка 52 микроарксекунд. Работа была опубликована в журнале New Astronomy.

"Понятие "черная дыра" для теоретика и наблюдателя отличается, – поясняет ведущий научный сотрудник лаборатории физики плазмы и астрофизики НИЦ "Курчатовский институт" Александр Захаров (в 2005 г. – сотрудник ИТЭФ). – *Для теоретика черная дыра – это определенная метрика, описывающая пространство-*

https://www.gazeta.ru/science/news/2022/06/15/17937578.shtml

- 15 июня 2022, 16:03
- **Сбылось предсказание российского ученого о загадочной тени**
- Борис Ганьжин
-
- Первое изображение сверхмассивной черной дыры в центре Млечного Пути, о получении которого в мае 2022 года **сообщила** коллаборация Телескопа горизонта событий Event Horizon Telescope, послужило подтверждением предсказания ведущего научного сотрудника лаборатории физики плазмы и астрофизики ККТЭФ НИЦ «Курчатовский институт» Александра Захарова и его итальянских коллег, сделанного в 2005 году. Об этом «Газете.Ru» сообщили в НИЦ «Курчатовский институт».

For about 20 years we declared black holes (for theorists) are dark spots (shadows) for observers

Available online at www.sciencedirect.com
SCIENCE DIRECT®
New Astronomy 10 (2005) 479–489
New Astronomy
www.elsevier.com/locate/newast

Measuring the black hole parameters in the galactic center with RADIOASTRON

A.F. Zakharov [a,b,c,*], A.A. Nucita [d], F. DePaolis [d], G. Ingrosso [d]

[a] Institute of Theoretical and Experimental Physics, 25, B. Cheremushkinskaya st., Moscow 117259, Russia
[b] Space Research Centre of Lebedev Physics Institute, Moscow, Russia
[c] Joint Institute for Nuclear Research, Dubna, Russia
[d] Dipartimento di Fisica, Universita di Lecce and INFN, Sezione di Lecce, Italy

Received 19 January 2005; accepted 21 February 2005
Available online 23 March 2005
Communicated by F. Melchiorri

Abstract

Recently, Holz and Wheeler (2002) [ApJ 578, 330] considered a very attracting possibility to detect retro-MACHOs, i.e., retro-images of the Sun by a Schwarzschild black hole. In this paper, we discuss glories (mirages) formed near rapidly rotating Kerr black hole horizons and propose a procedure to measure masses and rotation parameters analyzing these forms of mirages. In some sense that is a manifestation of gravitational lens effect in the strong gravitational field near black hole horizon and a generalization of the retro-gravitational lens phenomenon. We analyze the case of a Kerr black hole rotating at arbitrary speed for some selected positions of a distant observer with respect to the equatorial plane of a Kerr black hole. Some time ago Falcke, Melia, Agol (2000) [ApJ 528, L13S] suggested to search shadows at the Galactic Center. In this paper, we present the boundaries for shadows. We also propose to use future radio interferometer RADIOASTRON facilities to measure shapes of mirages (glories) and to evaluate the black hole spin as a function of the position angle of a distant observer.

PACS: 97.60.L; 04.70; 95.30.S; 04.20; 98.62.S

Keywords: Black hole physics; Gravitational lenses; Microlensing

1. Introduction

Recently Holz and Wheeler (2002) have suggested that a Schwarzschild black hole may form retro-images (called retro-MACHOs) if it is illuminated by the Sun. We analyze a rapidly rotating

* Corresponding author. Tel.:+7 095 1299759; fax: +7 095 8839601.
E-mail address: zakharov@itep.ru (A.F. Zakharov).

1384-1076/$ - see front matter © 2005 Elsevier B.V. All rights reserved.
doi:10.1016/j.newast.2005.02.007

ELSEVIER

New Astronomy
Top Cited Article 2005-2010

Awarded to:

Zakharov, A.F., Nucita, A.A., Depaolis, F., Ingrosso, G.

For the paper entitled:

"Measuring the black hole parameters in the galactic center with RADIOASTRON"

This paper was published in:

New Astronomy, Volume 10, Issue 6, 2005

David Clark
Senior Vice President, Physical Sciences I
Amsterdam, The Netherlands

Our proposal

In 2004-2005 we proposed a way to test GR predictions with Radioastron:

Since angular resolution of Radioastron at 1.3 cm is around 8 uas and the size of darkness (shadow) could help us to evaluate a charge, while shape could help us to evaluate a spin (good!)

The shortest wavelength is 1.3 cm (it is too long to detect shadow) (not good for Radioastron!)

So, we propose to test GR predictions about shape and size of BH images with observations. Astronomy is dealing with images. Therefore, establishing the correspondence of theoretical image and reconstructed image using observational data is an aim for further observations.

AFZ et al., NA (2005): “In our old paper
https://ui.adsabs.harvard.edu/.../2005NewA...10.../abstract
we wrote at the end "In spite of the difficulties of measuring the shapes of images near black holes is so attractive challenge to look at the ‘‘faces’’ of black holes because namely the mirages outline the ‘‘faces’’ and
correspond to fully general relativistic description of a region near black hole horizon without any assumption about a specific model for astrophysical processes around black holes (of course we assume that there are sources illuminating black hole surroundings). No doubt that the rapid growth of observational facilities will give a chance to measure the mirage shapes using not only RADIOASTRON facilities but using also other instruments and spectral bands (for example, X-ray interferometer MAXIM (White, 2000; Cash et al., 2000) or sub-mm VLBI array (Miyoshi, 2004)). Astro Space Centre of Lebedev Physics Institute proposed except the RADIOASTRON mission and developed also space based interferometers (Millimetron and Sub-millimetron) for future observations in mm and sub-mm bands. These instruments could be used for the determination of shadow shapes."

Measuring the black hole parameters in the Galactic Center with Radioastron

- Let us consider an illumination of black holes. Then retro-photons form caustics around black holes or mirages around black holes or boundaries around shadows.
- (Zakharov, Nucita, DePaolis, Ingrosso,
- New Astronomy 10 (2005) 479; astro-ph/0411511)

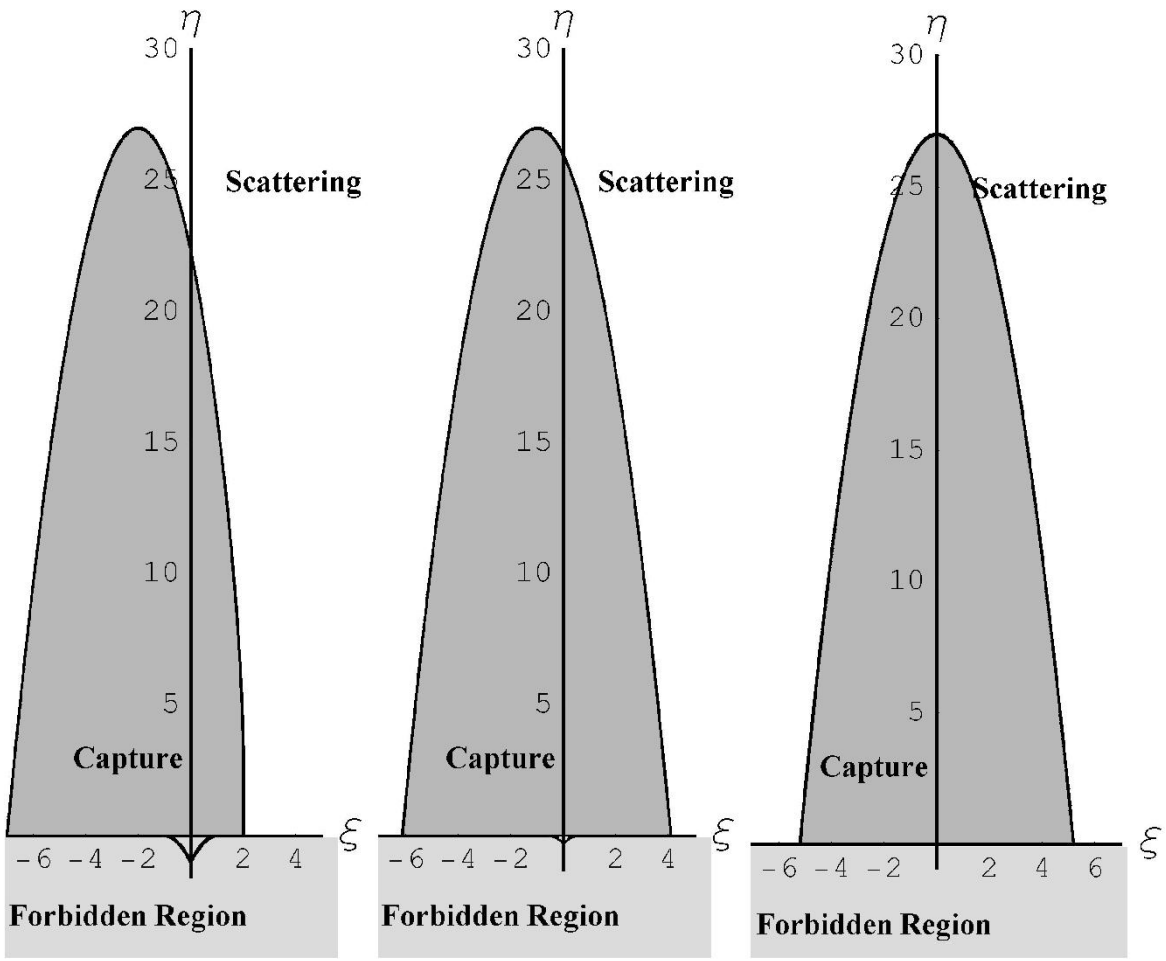

Fig. 1. Different types for photon trajectories and spin parameters ($a = 1., a = 0.5, a = 0.$). Critical curves separate capture and scatter regions. Here we show also the forbidden region corresponding to constants of motion $\eta < 0$ and $(\xi, \eta)\ \bar{\in}\ M$ as it was discussed in the text.

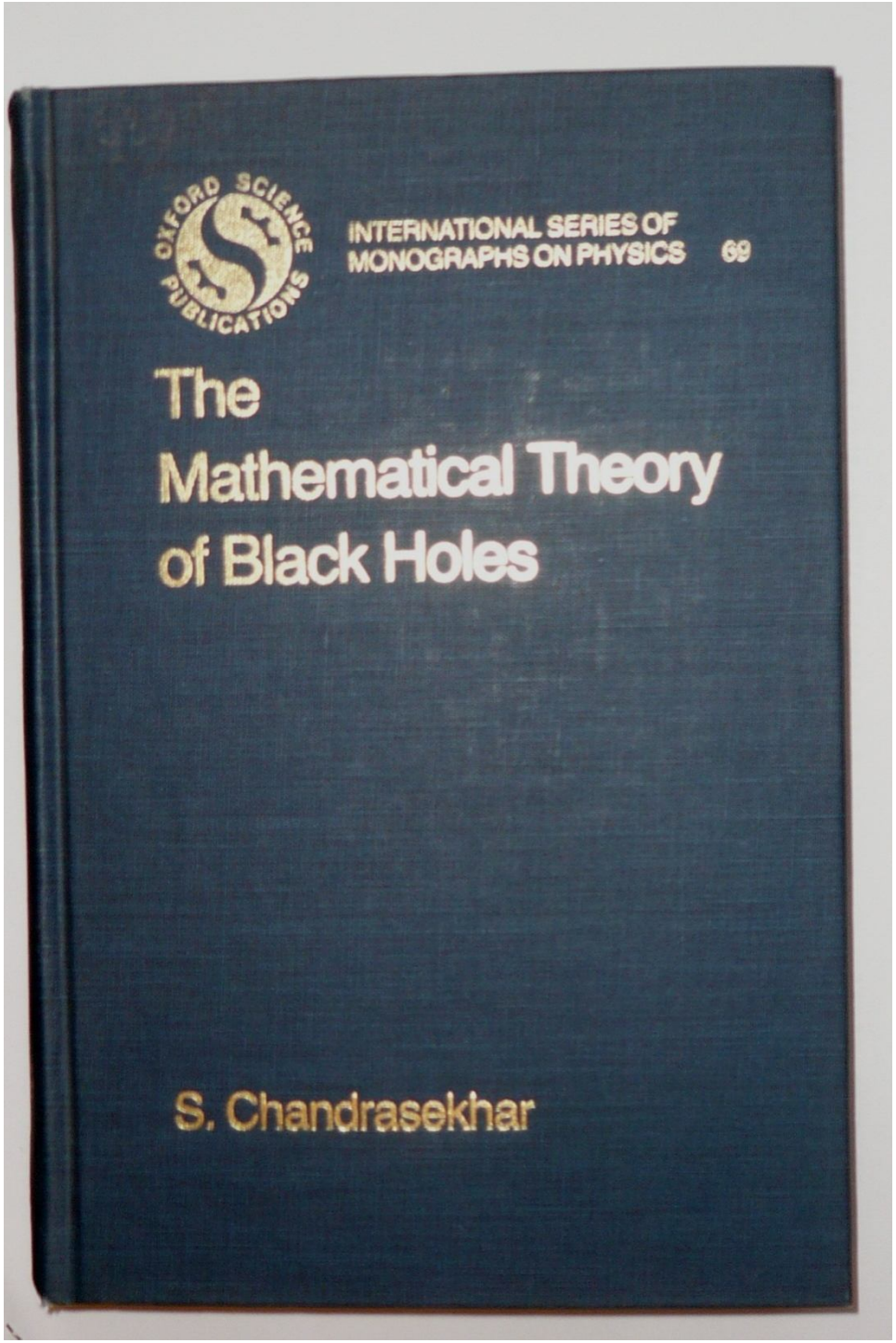
OXFORD SCIENCE PUBLICATIONS
INTERNATIONAL SERIES OF MONOGRAPHS ON PHYSICS 69
The Mathematical Theory of Black Holes
S. Chandrasekhar

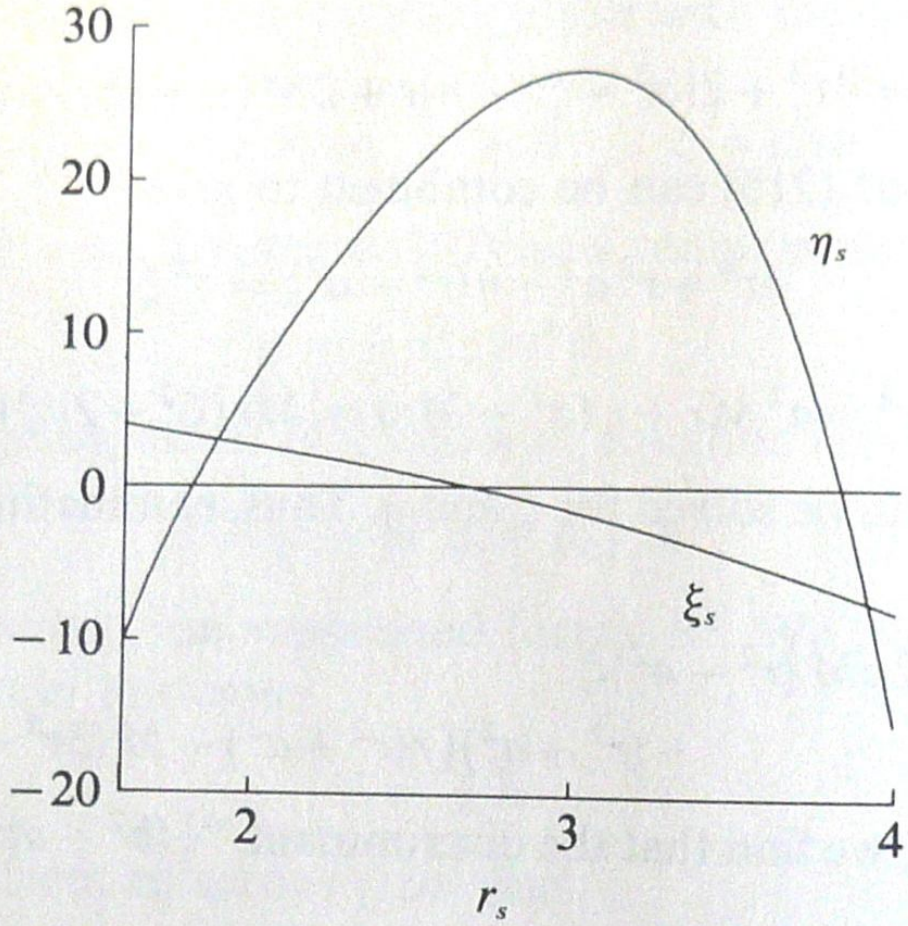

FIG. 34. The locus (ξ_s, η_s) determining the constants of the motion for three-dimensional orbits of constant radius described around a Kerr black-hole with $a = 0.8$. The unit of length along the abscissa is M.

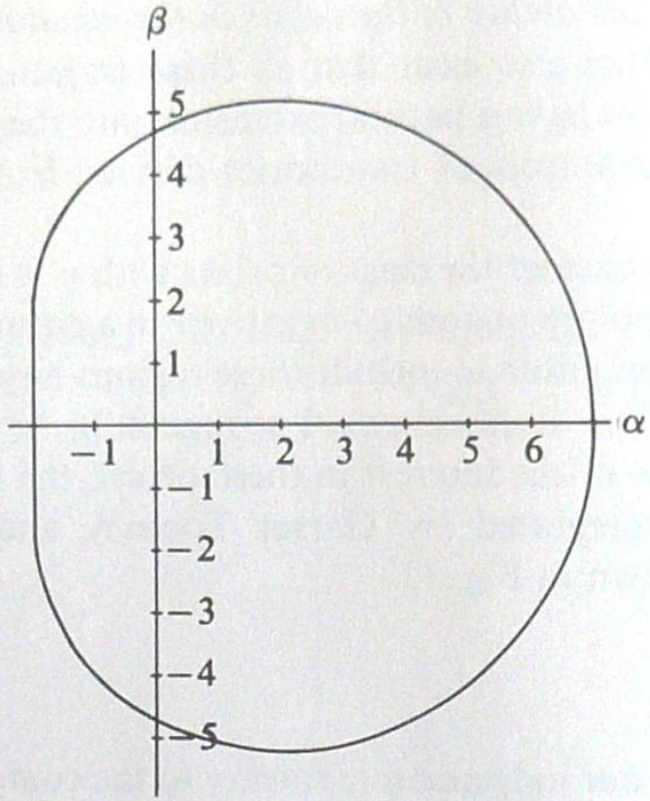

FIG. 38. The apparent shape of an extreme ($a = M$) Kerr black-hole as seen by a distant observer in the equatorial plane, if the black hole is in front of a source of illumination with an angular size larger than that of the black hole. The unit of length along the coordinate axes α and β (defined in equation (241) is M.

black hole from infinity, the apparent shape will be determined by

$$(\alpha, \beta) = [\xi, \sqrt{\eta(\xi)}]. \tag{242}$$

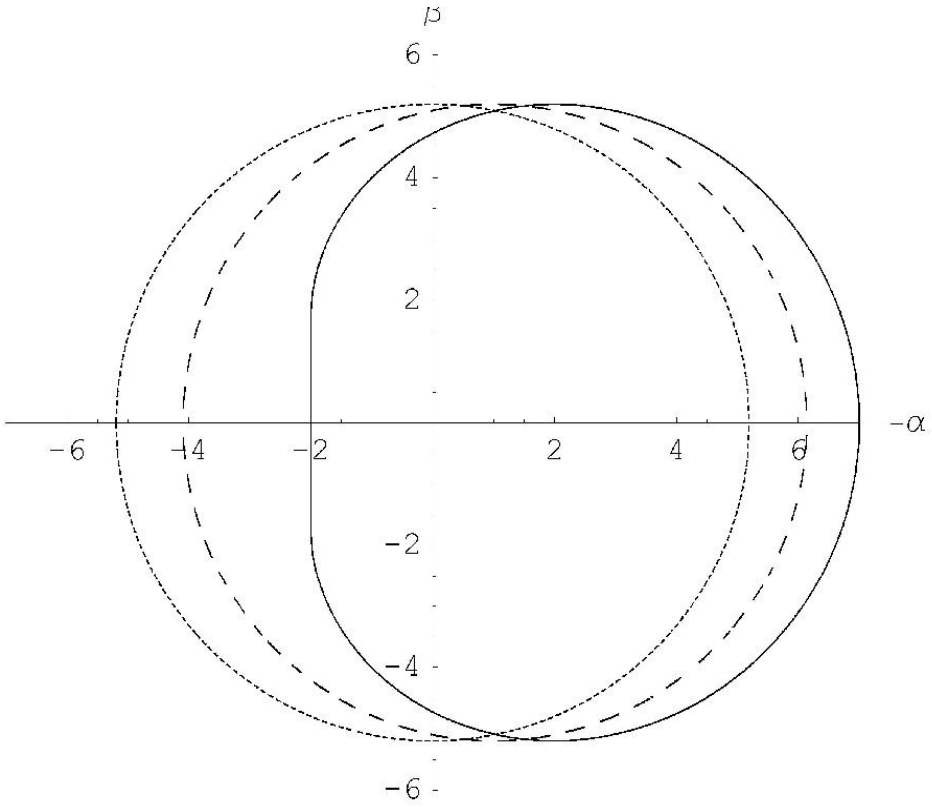

Fig. 2. Mirages around black hole for equatorial position of distant observer and different spin parameters. The solid line, the dashed line and the dotted line correspond to $a = 1, a = 0.5, a = 0$ correspondingly

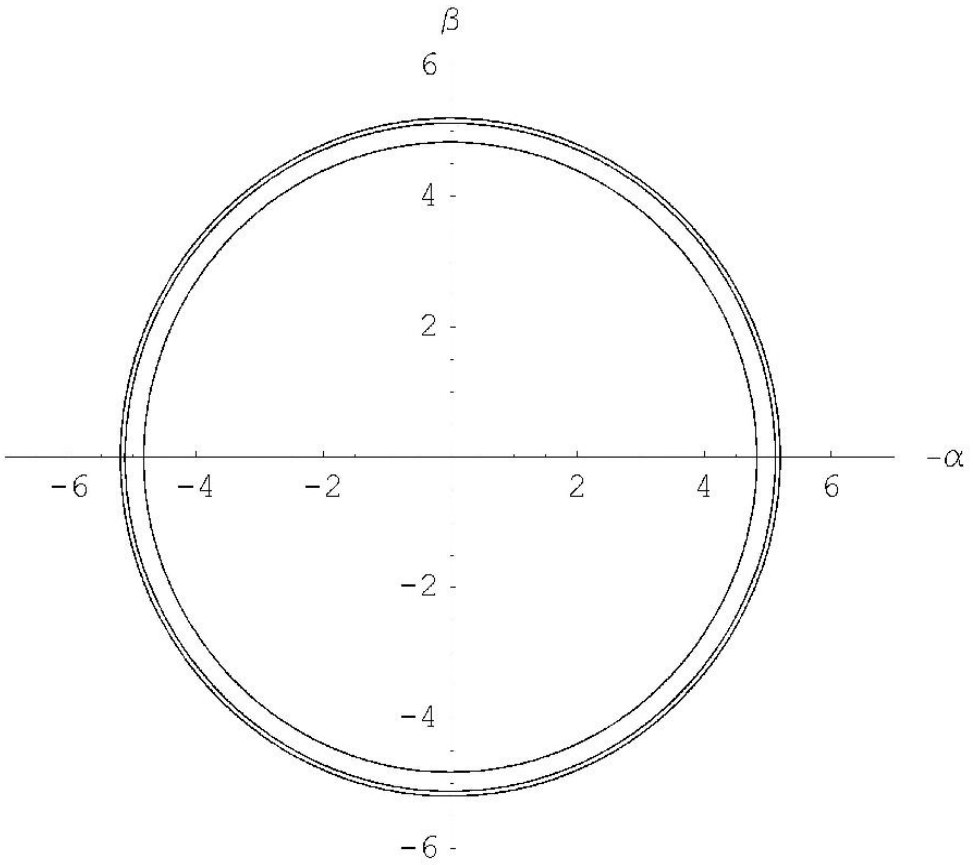

Fig. 3. Mirages around a black hole for the polar axis position of distant observer and different spin parameters ($a = 0, a = 0.5, a = 1$). Smaller radii correspond to greater spin parameters.

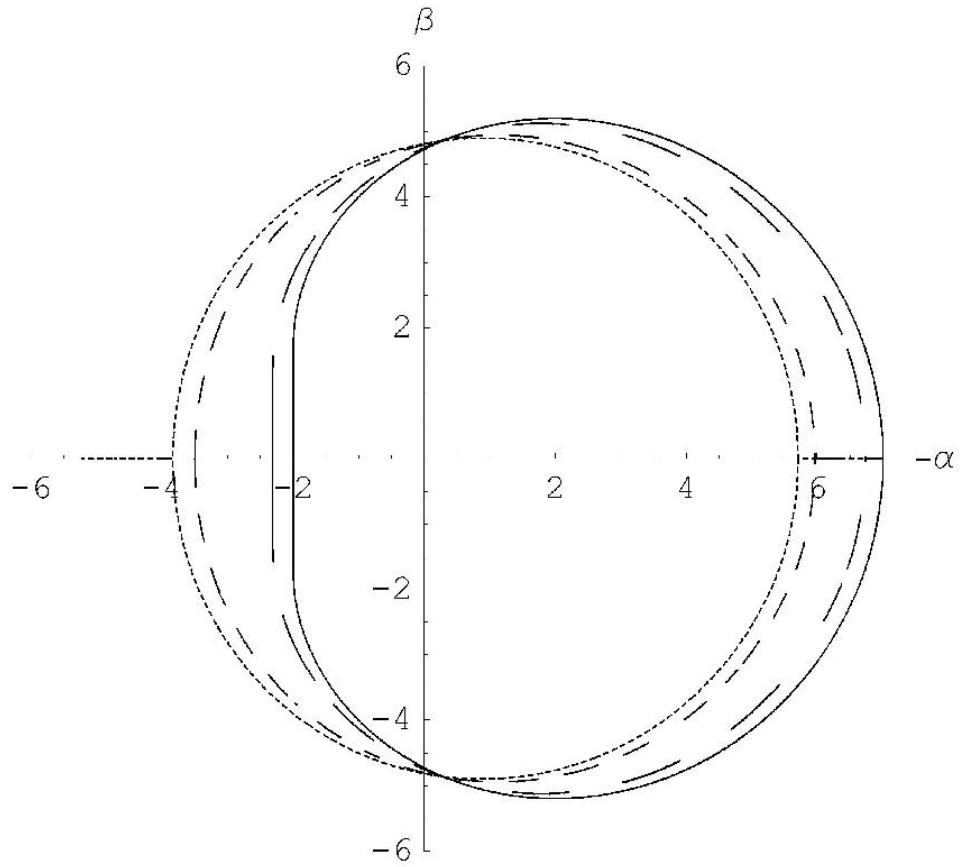

Fig. 5. Mirages around black hole for different angular positions of a distant observer and the spin $a = 1$. Solid, long dashed, short dashed and dotted lines correspond to $\theta_0 = \pi/2, \pi/3, \pi/6$ and $\pi/8$, respectively.

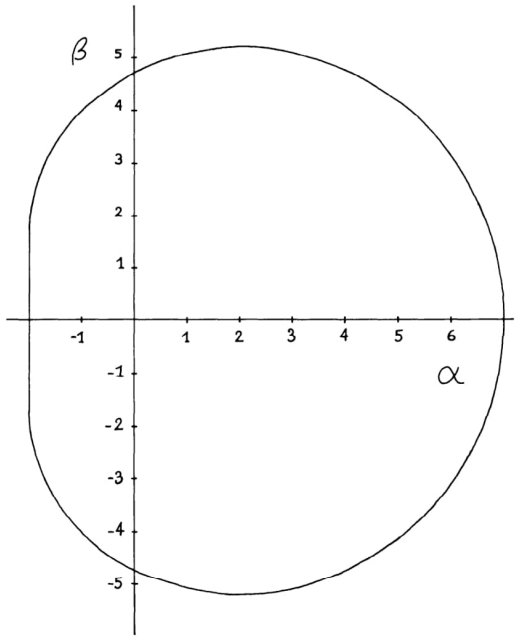

Figure 6. The apparent shape of an extreme ($a = m$) Kerr black hole as seen by a distant observer in the equatorial plane, if the black hole is in front of a source of illumination with an angular size larger than that of the black hole.

is largest there and because of the gravitational focusing effects associated with the bending of the rays toward the equatorial plane. Note that the radiation comes out along the flat portion of the apparent boundary of the extreme black hole as plotted in Figure 6.

D. Geometrical Optics

A detailed calculation of the brightness distribution coming from a source near a Kerr black hole requires more of geometrical optics than the calculation of photon trajectories. I will now review some techniques which are useful in making astrophysical calculations in connection with black holes.

The fundamental principle can be expressed as the conservation of photon density in phase space along each photon trajectory. A phase space element $d^3x\, d^3p$, the product of a proper spatial volume element and a physical momentum-space volume element in a local observer's frame of reference, is a Lorentz invariant, so the particular choice of local observer is arbitrary. The density $N(x^a, p^{(\beta)})$ is defined

James Maxwell Bardeen passed away on June 20, 2022

John Bardeen (1908 -1991), the father of J. M. Bardeen.
E. Wigner was J. Bardeen' supervisor

Direct Measurements of Black Hole Charge with Future Astrometrical Missions

A.F. Zakharov[1,2,3], F. De Paolis[4], G. Ingrosso[4], A.A. Nucita[4]

[1] Institute of Theoretical and Experimental Physics, 25, B.Cheremushkinskaya st., Moscow, 117259, Russia,

[2] Astro Space Centre of Lebedev Physics Institute, 84/32, Profsoyuznaya st., Moscow, 117810, Russia,

[3] Joint Institute for Nuclear Research, Dubna, Russia

[4] Department of Physics, University of Lecce and INFN, Section of Lecce, Via Arnesano, I-73100 Lecce, Italy

Received / accepted

Abstract. Recently, Zakharov et al. (2005a) considered the possibility of evaluating the spin parameter and the inclination angle for Kerr black holes in nearby galactic centers by using future advanced astrometrical instruments. A similar approach which uses the characteristic properties of gravitational retro-lensing images can be followed to measure the charge of Reissner-Nordström black hole. Indeed, in spite of the fact that their formation might be problematic, charged black holes are objects of intensive investigations. From the theoretical point of view it is well-known that a black hole is described by only three parameters, namely, its mass M, angular momentum J and charge Q. Therefore, it would be important to have a method for measuring all these parameters, preferably by model independent way. In this paper, we propose a procedure to measure the black hole charge by using the size of the retro-lensing images that can be revealed by future astrometrical missions. A discussion of the Kerr-Newmann black hole case is also offered.

Table 1. The fringe sizes (in micro arcseconds) for the standard and advanced apogees $B_{\max}$ (350 000 and 3 200 000 km, respectively).

$B_{\max}$(km)\λ(cm)	92	18	6.2	1.35
3.5×10^5	540	106	37	8
3.2×10^6	59	12	4	0.9

4. The space RADIOASTRON interferometer

The space-based radio telescope RADIOASTRON[1] is planned to be launched within few next years[2]. This space-based 10-m radio telescope will be used for space – ground VLBI observations. The measurements will have extremely high angular resolutions, namely about 1–10 μas (in particular about 8 μas at the shortest wavelength of 1.35 cm and a standard orbit[3], and could be about 0.9 μas for the high orbit configuration at the same wavelength. Four wave bands will be used corresponding to $\lambda = 1.35$ cm, $\lambda = 6.2$ cm, $\lambda = 18$ cm, $\lambda = 92$ cm (see Table 1). A detailed calculation of the high-apogee evolving orbits ($B_{\max}$) can be done, once the exact launch time is known.

After several years of observations, it should be possible to move the spacecraft to a much higher orbit (with apogee radius about 3.2 million km), by additional spacecraft maneuvering using the gravitational force of the Moon. The fringe sizes (in μas) for the apogee of the above-mentioned orbit and for all RADIOASTRON wavelengths are given in Table 1.

By comparing Figs. 1, 2 and Table 1, one can see that there are non-negligible chances to observe such mirages around the black hole at the Galactic Center and in nearby AGNs and microquasars in the radio-band using RADIOASTRON facilities.

We also mention that this high resolution in radio band will be achieved also by Japanese VLBI project VERA (VLBI Exploration of Radio Astrometry), since the angular resolution aimed at will be at the 10 μas level (Sawad-Satoh 2000; Honma 2001). Therefore, the only problem left is to have a powerful enough radio source to illuminate a black hole in order to have retro-lensing images detectable by such radio VLBI telescopes as RADIOASTRON or VERA.

[1] See web-site `http://www.asc.rssi.ru/radioastron/` for more information.

[2] This project was proposed by the Astro Space Center (ASC) of Lebedev Physical Institute of the Russian Academy of Sciences (RAS) in collaboration with other institutions of RAS and RosAviaKosmos. Scientists from 20 countries are developing the scientific payload for the satellite by providing by ground-based support to the mission.

[3] The satellite orbit will have high apogee, and its rotation period around Earth will be 9.5 days, which evolves as a result of the weak gravitational perturbations from the Moon and the Sun. The perigee has been planned to be between 10^4 and 7×10^4 km and the apogee between 310 and 390 thousand kilometers. The basic orbit parameters will be the following: the orbital period is $P = 9.5$ days, the semi-major axis is $a = 189\,000$ km, the eccentricity is $e = 0.853$, the perigee is $H = 29\,000$ km.

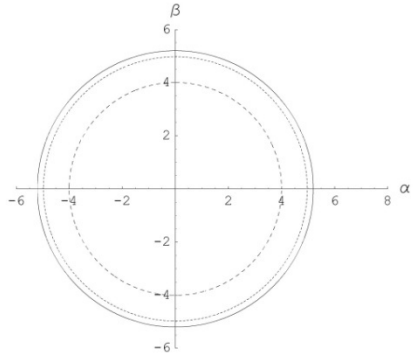

Fig. 1. Shadow (mirage) sizes are shown for selected charges of black holes $Q = 0$ (solid line), $Q = 0.5$ (short dashed line), and $Q = 1$ (long dashed line).

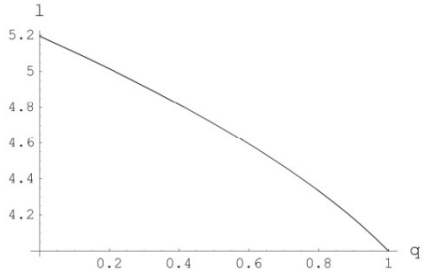

Fig. 2. The mirage radius l is shown as a function of the black hole charge q (l and q are given in units of M).

5. Searches for mirages near Sgr A^* with RADIOASTRON

Radio, near-infrared, and X-ray spectral band observations are developing very rapidly (Lo et al. 1998, 1999; Genzel et al. 2003; Ghez et al. 2004; Baganoff et al. 2001, 2003; Bower et al. 2002, 2003; Narayan 2003; Bower et al. 2004)[4], and it is known that Sgr A^* harbors the closest massive black hole with mass estimated to be 4.07×10^6 $M_\odot$ (Bower et al. 2004; Melia & Falcke 2001; Ghez et al. 2003; Schodel et al. 2003).

Following the idea of Falcke et al. (2000) and of Zakharov et al. (2005a,b,c,d) we propose to use the VLBI technique to observe mirages around massive black holes and, in particular, towards the black hole at Galactic Center. To evaluate the shadow shape Falcke et al. (2000) used the ray-tracing technique. The boundaries of the shadows are black hole mirages.

[4] An interesting idea to use radio pulsars to investigate the region nearby black hole horizon was proposed recently by Pfahl & Loeb (2003).

PHYSICAL REVIEW D **90,** 062007 (2014)

Constraints on a charge in the Reissner-Nordström metric for the black hole at the Galactic Center

Alexander F. Zakharov*

North Carolina Central University, Durham, North Carolina 27707, USA; Institute of Theoretical and Experimental Physics, Moscow 117218, Russia; Joint Institute for Nuclear Research, Dubna 141980, Russia; Institute for Computer Aided Design of RAS, 123056 Moscow, Russia; and National Research Nuclear University (NRNU MEPHI), 115409 Moscow, Russia

(Received 5 March 2013; published 9 September 2014)

Using an algebraic condition of vanishing discriminant for multiple roots of fourth-degree polynomials, we derive an analytical expression of a shadow size as a function of a charge in the Reissner-Nordström (RN) metric [1,2]. We consider shadows for negative tidal charges and charges corresponding to naked singularities $q = \mathcal{Q}^2/M^2 > 1$, where $\mathcal{Q}$ and M are black hole charge and mass, respectively, with the derived expression. An introduction of a negative tidal charge q can describe black hole solutions in theories with extra dimensions, so following the approach we consider an opportunity to extend the RN metric to negative $\mathcal{Q}^2$, while for the standard RN metric $\mathcal{Q}^2$ is always non-negative. We found that for $q > 9/8$, black hole shadows disappear. Significant tidal charges $q = -6.4$ (suggested by Bin-Nun [3–5]) are not consistent with observations of a minimal spot size at the Galactic Center observed in mm-band; moreover, these observations demonstrate that a Reissner-Nordström black hole with a significant charge $q \approx 1$ provides a better fit of recent observational data for the black hole at the Galactic Center in comparison with the Schwarzschild black hole.

DOI: 10.1103/PhysRevD.90.062007 PACS numbers: 04.80.Cc, 04.20.-q, 04.50.Gh, 04.70.Bw

I. INTRODUCTION

Soon after the discovery of general relativity (GR), the first solutions corresponding to spherical symmetric black holes were found [1,2,6]; however, initially people were rather sceptical about possible astronomical applications of the solutions corresponding to black holes [7] (see also, for instance, one of the first textbooks on GR [8]). Even after an introduction to the black hole concept by Wheeler [9] (he used the term in his public lecture in 1967 [10]), we did not know too many examples where we really need GR models with strong gravitational fields that arise near black hole horizons to explain observational data. The cases where we need strong field approximation are very important since they give an opportunity to check GR predictions in a strong field limit; therefore, one could significantly constrain alternative theories of gravity.

One of the most important options to test gravity in the strong field approximation is analysis of relativistic line shape as it was shown in [11], with assumptions that a line emission is originated at a circular ring area of a flat accretion disk. Later on, such signatures of the Fe $K\alpha$ line have been found in the active galaxy MCG-6-30-15 [12]. Analyzing the spectral line shape, the authors concluded the emission region is so close to the black hole horizon that one has to use Kerr metric approximation [13] to fit observational data [12]. Results of simulations of iron $K\alpha$ line formation are given in [14,15] (where we used our approach [16]); see also [17] for a more recent review of the subject.

Now there are two basic observational techniques to investigate a gravitational potential at the Galactic Center, namely, (a) monitoring the orbits of bright stars near the Galactic Center to reconstruct a gravitational potential [18] (see also a discussion about an opportunity to evaluate black hole dark matter parameters in [19] and an opportunity to constrain some class of an alternative theory of gravity [20]) and (b) measuring in mm band, with VLBI technique, the size and shape of shadows around the black hole, giving an alternative possibility to evaluate black hole parameters. The formation of retro-lensing images (also known as mirages, shadows, or "faces" in the literature) due to the strong gravitational field effects nearby black holes has been investigated by several authors [21–24].

Theories with extra dimensions admit astrophysical objects (supermassive black holes in particular) which are rather different from standard ones. Tests have been proposed when it would be possible to discover signatures of extra dimensions in supermassive black holes since the gravitational field may be different from the standard one in the GR approach. So, gravitational lensing features are different for alternative gravity theories with extra dimensions and general relativity.

Recently, Bin-Nun [3–5] discussed the possibility that the black hole at the Galactic Center is described by the tidal Reissner-Nordström metric which may be admitted by the Randall-Sundrum II braneworld scenario [25]. Bin-Nun suggested an opportunity of evaluating the black hole

*zakharov@itep.ru

$$\mathrm{Dis}(s_1,s_2,s_3,s_4)=\begin{vmatrix}1 & 1 & 1 & 1\\ X_1 & X_2 & X_3 & X_4\\ X_1^2 & X_2^2 & X_3^2 & X_4^2\\ X_1^3 & X_2^3 & X_3^3 & X_4^3\end{vmatrix}^2 = \begin{vmatrix}4 & p_1 & p_2 & p_3\\ p_1 & p_2 & p_3 & p_4\\ p_2 & p_3 & p_4 & p_5\\ p_3 & p_4 & p_5 & p_6\end{vmatrix}. \quad (20)$$

Expressing the polynomials $p_k(1\le k\le 6)$ in terms of the polynomials $s_k(1\le k\le 4)$ and using Newton's equations we calculate the polynomials and discriminant of the family X_1,X_2,X_3,X_4 in roots of the polynomial $R(r)$; we obtain

$$p_1=s_1=0,\qquad p_2=-2s_2,\qquad p_3=3s_3,$$
$$p_4=2s_2^2-4s_4,\qquad p_5=-5s_3s_2,$$
$$p_6=-2s_2^3+3s_3^2+6s_4s_2, \quad (21)$$

where $s_1=0, s_2=-l, s_3=-2l, s_4=-ql$, corresponding to the polynomial $R(r)$ in Eq. (8). The discriminant Dis of the polynomial $R(r)$ has the form

$$\mathrm{Dis}(s_1,s_2,s_3,s_4)=\begin{vmatrix}4 & 0 & 2l & -6l\\ 0 & 2l & -6l & 2l(l+2q)\\ 2l & -6l & 2l(l+2q) & -10l^2\\ -6l & 2l(l+2q) & -10l^2 & 2l^2(l+6+3q)\end{vmatrix}$$
$$=16l^3[l^2(1-q)+l(-8q^2+36q-27)-16q^3]. \quad (22)$$

The polynomial $R(r)$ thus has a multiple root if and only if

$$l^3[l^2(1-q)+l(-8q^2+36q-27)-16q^3]=0. \quad (23)$$

Excluding the case $l=0$, which corresponds to a multiple root at $r=0$, we find that the polynomial $R(r)$ has a multiple root for $r\ge r_+$ if and only if

$$l^2(1-q)+l(-8q^2+36q-27)-16q^3=0. \quad (24)$$

If $q=0$, we obtain the well-known result for a Schwarzschild black hole [38,39,49], $l_{\rm cr}=27$, or $\xi_{\rm cr}=3\sqrt{3}$ [where $l_{\rm cr}$ is the positive root of Eq. (24)]. If $q=1$, then $l=16$, or $\xi_{\rm cr}=4$, which also corresponds to numerical results given in paper [50]. The photon capture cross section for an extreme charged black hole turns out to be considerably smaller than the capture cross section of a Schwarzschild black hole. The critical value of the impact parameter, characterizing the capture cross section for a RN black hole, is determined by the equation

$$l_{\rm cr}=\frac{(8q^2-36q+27)+\sqrt{D_1}}{2(1-q)}, \quad (25)$$

where $D_1=(8q^2-36q+27)^2+64q^3(1-q)=-512(q-\frac{9}{8})^3$. It is clear from the last relation that there are circular unstable photon orbits only for $q\le\frac{9}{8}$ (see also results in [37] about the same critical value). Substituting Eq. (25) into the expression for the coefficients of the polynomial $R(r)$ it is easy to calculate the radius of the unstable circular photon orbit (which is the same as the minimum periastron distance). The orbit of a photon moving from infinity with the critical impact parameter, determined in accordance with Eq. (25) spirals into circular orbit. To find a radius of photon unstable orbit we will solve Eq. (7) substituting $l_{\rm cr}$ in the relation. From trigonometric formula for roots of cubic equation we have

$$r_{\rm crit}=2\sqrt{\frac{l_{\rm cr}}{6}}\cos\frac{\alpha}{3}, \quad (26)$$

where

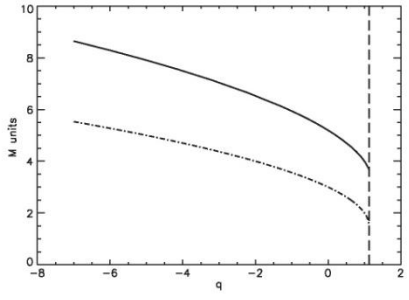

FIG. 1. Shadow (mirage) radius (solid line) and radius of the last circular unstable photon orbit (dot-dashed line) in M units as a function of q. The critical value $q=9/8$ is shown with dashed vertical line.

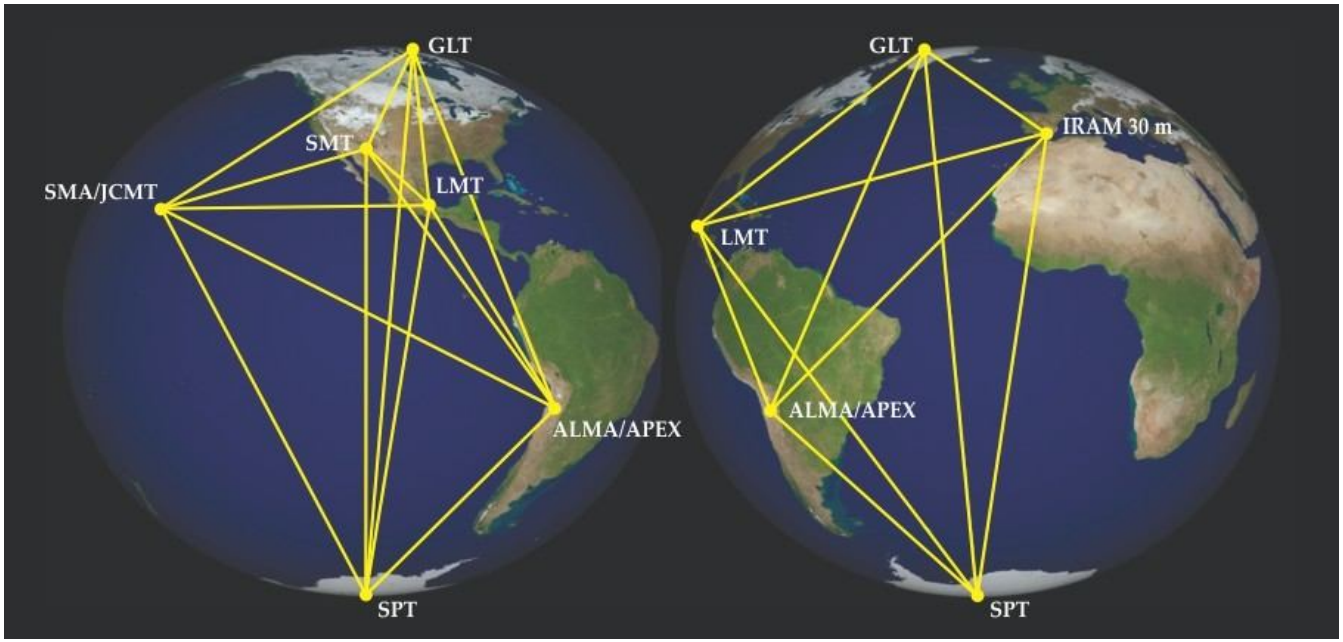

Figure 2. ***The Event Horizon Telescope*** *is a global array of millimeter telescopes (see http://eventhorizontelescope.org/array) that aims to take the first pictures of black holes. (Courtesy of Dan Marrone/University of Arizona.)*

Published in: Dimitrios Psaltis; Feryal Özel; *Physics Today* **2018,** 71, 70-71.
DOI: 10.1063/PT.3.3906

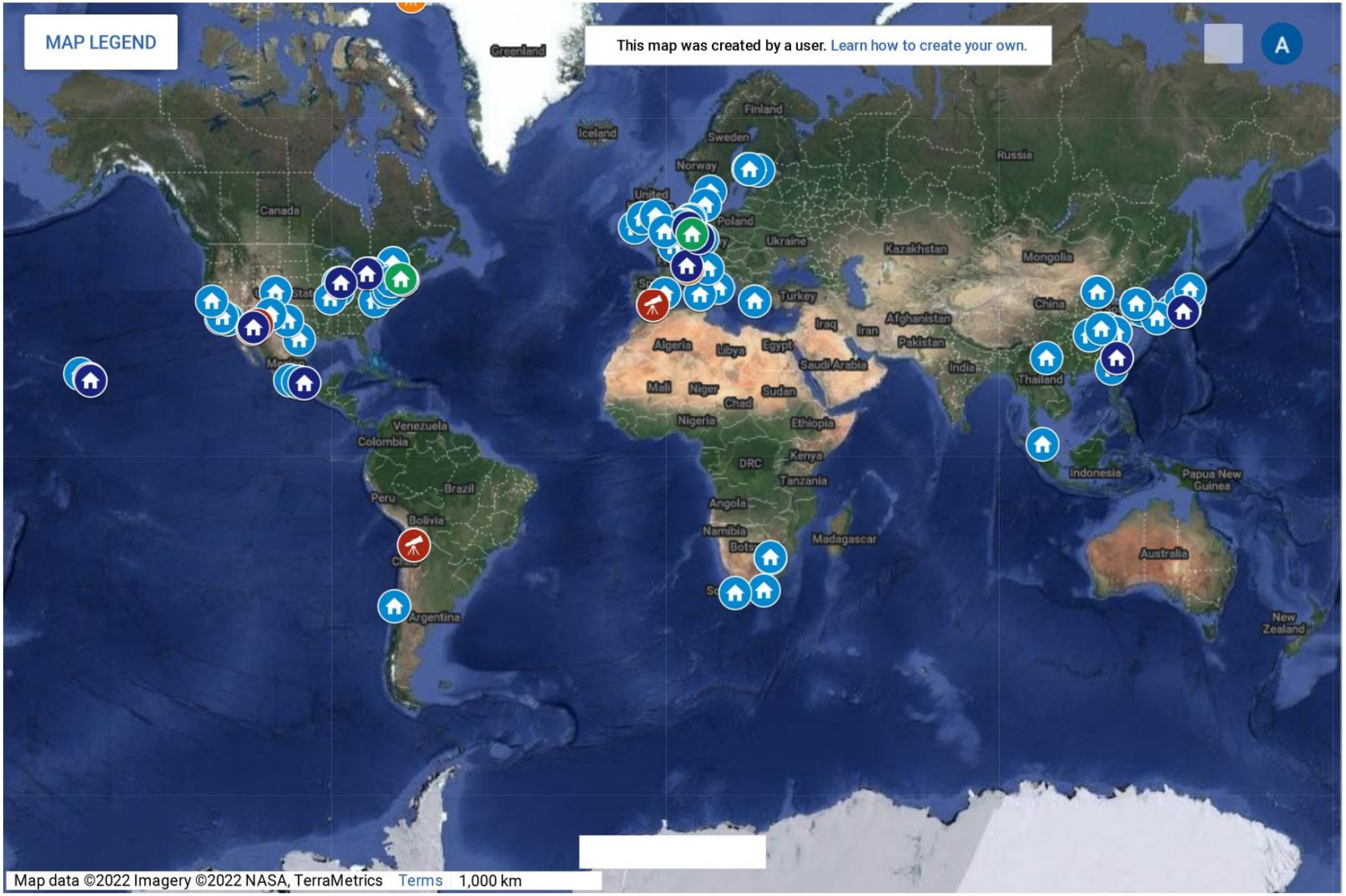
MAP LEGEND
This map was created by a user. Learn how to create your own.
A
Greenland
Iceland
Finland
Sweden
Norway
Russia
Canada
Poland
Ukraine
Kazakhstan
Mongolia
Turkey
China
Iraq
Iran
Afghanistan
Pakistan
Algeria
Libya
Egypt
Saudi Arabia
India
Thailand
Mali
Niger
Sudan
Chad
Nigeria
Ethiopia
Venezuela
Colombia
Kenya
DRC
Tanzania
Indonesia
Papua New Guinea
Brazil
Peru
Angola
Bolivia
Namibia
Madagascar
Australia
Argentina
New Zealand
Map data ©2022 Imagery ©2022 NASA, TerraMetrics
Terms
1,000 km

EHT team: “Similarly, for the EHT, the data we take only tells us only a piece of the story, as there are an infinite number of possible images that are perfectly consistent with the data we measure. But not all images are created equal— some look more like what we think of as images than others. To chose the best image, we essentially take all of the infinite images that explain our telescope measurements, and rank them by how reasonable they look. We then choose the image (or set of images) that looks most reasonable. “

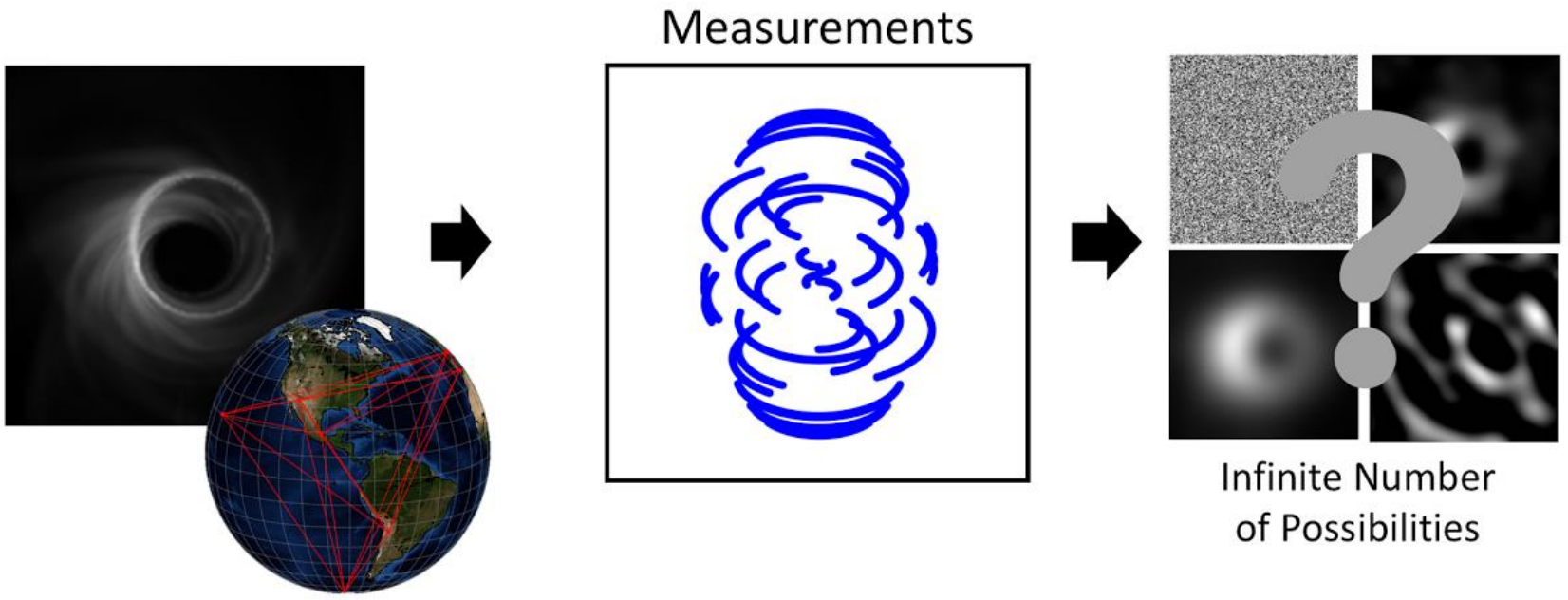

Constraints on black-hole charges with the 2017 EHT observations of M87*

Prashant Kocherlakota,[1] Luciano Rezzolla,[1–3] Heino Falcke,[4] Christian M. Fromm,[5,6,1] Michael Kramer,[7] Yosuke Mizuno,[8,9] Antonios Nathanail,[9,10] Héctor Olivares,[4] Ziri Younsi,[11,9] Kazunori Akiyama,[12,13,5] Antxon Alberdi,[14] Walter Alef,[7] Juan Carlos Algaba,[15] Richard Anantua,[5,6,16] Keiichi Asada,[17] Rebecca Azulay,[18,19,7] Anne-Kathrin Baczko,[7] David Ball,[20] Mislav Baloković,[5,6] John Barrett,[12] Bradford A. Benson,[21,22] Dan Bintley,[23] Lindy Blackburn,[5,6] Raymond Blundell,[6] Wilfred Boland,[24] Katherine L. Bouman,[5,6,25] Geoffrey C. Bower,[26] Hope Boyce,[27,28] Michael Bremer,[29] Christiaan D. Brinkerink,[4] Roger Brissenden,[5,6] Silke Britzen,[7] Avery E. Broderick,[30–32] Dominique Broguiere,[29] Thomas Bronzwaer,[4] Do-Young Byun,[33,34] John E. Carlstrom,[35,22,36,37] Andrew Chael,[38,39] Chi-kwan Chan,[20,40] Shami Chatterjee,[41] Koushik Chatterjee,[42] Ming-Tang Chen,[26] Yongjun Chen (陈永军),[43,44] Paul M. Chesler,[5] Ilje Cho,[33,34] Pierre Christian,[45] John E. Conway,[46] James M. Cordes,[41] Thomas M. Crawford,[22,35] Geoffrey B. Crew,[12] Alejandro Cruz-Osorio,[9] Yuzhu Cui,[47,48] Jordy Davelaar,[49,16,4] Mariafelicia De Laurentis,[50,9,51] Roger Deane,[52–54] Jessica Dempsey,[23] Gregory Desvignes,[55] Sheperd S. Doeleman,[5,6] Ralph P. Eatough,[56,7] Joseph Farah,[6,5,57] Vincent L. Fish,[12] Ed Fomalont,[58] Raquel Fraga-Encinas,[4] Per Friberg,[23] H. Alyson Ford,[59] Antonio Fuentes,[14] Peter Galison,[5,60,61] Charles F. Gammie,[62,63] Roberto García,[29] Olivier Gentaz,[29] Boris Georgiev,[31,32] Ciriaco Goddi,[4,64] Roman Gold,[65,30] José L. Gómez,[14] Arturo I. Gómez-Ruiz,[66,67] Minfeng Gu (顾敏峰),[43,68] Mark Gurwell,[6] Kazuhiro Hada,[47,48] Daryl Haggard,[27,28] Michael H. Hecht,[12] Ronald Hesper,[69] Luis C. Ho (何子山),[70,71] Paul Ho,[17] Mareki Honma,[47,48,72] Chih-Wei L. Huang,[17] Lei Huang (黄磊),[43,68] David H. Hughes,[66] Shiro Ikeda,[13,73–75] Makoto Inoue,[17] Sara Issaoun,[4] David J. James,[5,6] Buell T. Jannuzi,[20] Michael Janssen,[7] Britton Jeter,[31,32] Wu Jiang (江悟),[43] Alejandra Jimenez-Rosales,[4] Michael D. Johnson,[5,6] Svetlana Jorstad,[76,77] Taehyun Jung,[33,34] Mansour Karami,[30,31] Ramesh Karuppusamy,[7] Tomohisa Kawashima,[78] Garrett K. Keating,[6] Mark Kettenis,[79] Dong-Jin Kim,[7] Jae-Young Kim,[33,7] Jongsoo Kim,[33] Junhan Kim,[20,25] Motoki Kino,[13,80] Jun Yi Koay,[17] Yutaro Kofuji,[47,72] Patrick M. Koch,[17] Shoko Koyama,[17] Carsten Kramer,[29] Thomas P. Krichbaum,[7] Cheng-Yu Kuo,[81,17] Tod R. Lauer,[82] Sang-Sung Lee,[33] Aviad Levis,[25] Yan-Rong Li (李彦荣),[83] Zhiyuan Li (李志远),[84,85] Michael Lindqvist,[46] Rocco Lico,[14,7] Greg Lindahl,[6] Jun Liu (刘俊),[7] Kuo Liu,[7] Elisabetta Liuzzo,[86] Wen-Ping Lo,[17,87] Andrei P. Lobanov,[7] Laurent Loinard,[88,89] Colin Lonsdale,[12] Ru-Sen Lu (路如森),[43,44,7] Nicholas R. MacDonald,[7] Jirong Mao (毛基荣),[90–92] Nicola Marchili,[86,7] Sera Markoff,[42,93] Daniel P. Marrone,[20] Alan P. Marscher,[76] Iván Martí-Vidal,[18,19] Satoki Matsushita,[17] Lynn D. Matthews,[12] Lia Medeiros,[94,20] Karl M. Menten,[7] Izumi Mizuno,[23] James M. Moran,[5,6] Kotaro Moriyama,[12,47] Monika Moscibrodzka,[4] Cornelia Müller,[7,4] Gibwa Musoke,[42,4] Alejandro Mus Mejías,[18,19] Hiroshi Nagai,[13,48] Neil M. Nagar,[95] Masanori Nakamura,[96,17] Ramesh Narayan,[5,6] Gopal Narayanan,[97] Iniyan Natarajan,[54,52,98] Joseph Neilsen,[99] Roberto Neri,[29] Chunchong Ni,[31,32] Aristeidis Noutsos,[7] Michael A. Nowak,[100] Hiroki Okino,[47,72] Gisela N. Ortiz-León,[7] Tomoaki Oyama,[47] Feryal Özel,[20] Daniel C. M. Palumbo,[5,6] Jongho Park,[17] Nimesh Patel,[6] Ue-Li Pen,[30,101–103] Dominic W. Pesce,[5,6] Vincent Piétu,[29] Richard Plambeck,[104] Aleksandar PopStefanija,[97] Oliver Porth,[42,9] Felix M. Pötzl,[7] Ben Prather,[62] Jorge A. Preciado-López,[30] Dimitrios Psaltis,[20] Hung-Yi Pu,[105,17,30] Venkatessh Ramakrishnan,[95] Ramprasad Rao,[26] Mark G. Rawlings,[23] Alexander W. Raymond,[5,6] Angelo Ricarte,[5,6] Bart Ripperda,[106,16] Freek Roelofs,[4] Alan Rogers,[12] Eduardo Ros,[7] Mel Rose,[20] Arash Roshanineshat,[20] Helge Rottmann,[7] Alan L. Roy,[7] Chet Ruszczyk,[12] Kazi L. J. Rygl,[86] Salvador Sánchez,[107] David Sánchez-Arguelles,[66,67] Mahito Sasada,[47,108] Tuomas Savolainen,[109,110,7] F. Peter Schloerb,[97] Karl-Friedrich Schuster,[29] Lijing Shao,[7,71] Zhiqiang Shen (沈志强),[43,44] Des Small,[79] Bong Won Sohn,[33,34,111] Jason SooHoo,[12] He Sun (孙赫),[25] Fumie Tazaki,[47] Alexandra J. Tetarenko,[112] Paul Tiede,[31,32] Remo P. J. Tilanus,[4,64,113,20] Michael Titus,[12] Kenji Toma,[114,115] Pablo Torne,[7,107] Tyler Trent,[20] Efthalia Traianou,[7] Sascha Trippe,[116] Ilse van Bemmel,[79] Huib Jan van Langevelde,[79,117] Daniel R. van Rossum,[4] Jan Wagner,[7] Derek Ward-Thompson,[118] John Wardle,[119] Jonathan Weintroub,[5,6] Norbert Wex,[7] Robert Wharton,[7] Maciek Wielgus,[5,6] George N. Wong,[62] Qingwen Wu (吴庆文),[120] Doosoo Yoon,[42] André Young,[4] Ken Young,[6] Feng Yuan (袁峰),[43,68,121] Ye-Fei Yuan (袁业飞),[122] J. Anton Zensus,[7] Guang-Yao Zhao,[14] and Shan-Shan Zhao[43]

(EHT Collaboration)

[1]*Institut für Theoretische Physik, Goethe-Universität, Max-von-Laue-Strasse 1, 60438 Frankfurt, Germany*
[2]*Frankfurt Institute for Advanced Studies, Ruth-Moufang-Strasse 1, 60438 Frankfurt, Germany*
[3]*School of Mathematics, Trinity College, Dublin 2, Ireland*
[4]*Department of Astrophysics, Institute for Mathematics, Astrophysics and Particle Physics (IMAPP), Radboud University, P.O. Box 9010, 6500 GL Nijmegen, Netherlands*
[5]*Black Hole Initiative at Harvard University, 20 Garden Street, Cambridge, Massachusetts 02138, USA*

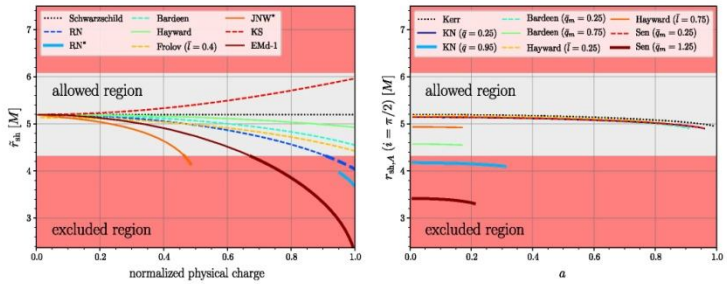

FIG. 2. Left: shadow radii $\tilde{r}_{sh}$ for various spherically symmetric black-hole solutions, as well as for the JNW and RN naked singularities (marked with an asterisk), as a function of the physical charge normalized to its maximum value. The gray/red shaded regions refer to the areas that are 1-σ consistent/inconsistent with the 2017 EHT observations and highlight that the latter set constraints on the physical charges (see also Fig. 3 for the EMd-2 black hole). Right: shadow areal radii $r_{sh,A}$ as a function of the dimensionless spin a for four families of black-hole solutions when viewed on the equatorial plane ($i=\pi/2$). Also in this case, the observations restrict the ranges of the physical charges of the Kerr-Newman and the Sen black holes (see also Fig. 3).

independent charges—can also produce shadow radii that are incompatible with the EHT observations; we will discuss this further below. The two EMd black-hole solutions (1 and 2) correspond to fundamentally different field contents, as discussed in [70].

We report in the right panel of Fig. 2 the shadow areal radius $r_{sh,A}$ for a number of stationary black holes, such as Kerr [72], Kerr-Newman (KN) [73], Sen [74], and the rotating versions of the Bardeen and Hayward black holes [75]. The data refers to an observer inclination angle of $i=\pi/2$, and we find that the variation in the shadow size with spin at higher inclinations (of up to $i=\pi/100$) is at most about 7.1% (for $i=\pi/2$, this is 5%); of course, at zero-spin the shadow size does not change with inclination. The shadow areal radii are shown as a function of the dimensionless spin of the black hole $a:=J/M^2$, where J is its angular momentum, and for representative values of the additional parameters that characterize the solutions. Note that—similar to the angular momentum for a Kerr black hole—the role of an electric charge or the presence of a de Sitter core (as in the case of the Hayward black holes) is to reduce the apparent size of the shadow. Furthermore, on increasing the spin parameter, we recover the typical trend that the shadow becomes increasingly noncircular, as encoded, e.g., in the distortion parameter δ_{sh} defined in [57,83] (see Appendix). Also in this case, while the regular rotating Bardeen and Hayward solutions are compatible with the present constraints set by the 2017 EHT observations, the Kerr-Newman and Sen families of black holes can produce shadow areal radii that lie outside of the 1-σ region allowed by the observations.

To further explore the constraints on the excluded regions for the Einstein-Maxwell-dilaton 2 and the Sen black holes, we report in Fig. 3 the relevant ranges for these two solutions. The Einstein-Maxwell-dilaton 2 black holes are nonrotating but have two physical charges expressed by the coefficients $0<\tilde{q}_e<\sqrt{2}$ and $0<\tilde{q}_m<\sqrt{2}$, while the Sen black holes spin (a) and have an additional electromagnetic charge $\tilde{q}_m$. Also in this case, the gray/red shaded regions refer to the areas that are consistent/inconsistent with the 2017 EHT observations. The figure shows rather easily that for these two black-hole families there are large

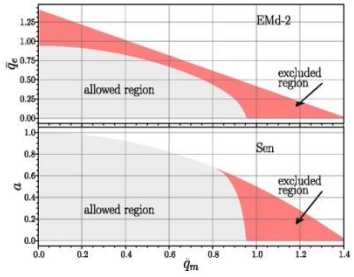

FIG. 3. Constraints set by the 2017 EHT observations on the nonrotating Einstein-Maxwell-dilaton 2 and on the rotating Sen black holes. Also in this case, the gray/red shaded regions refer to the areas that are 1-σ consistent/inconsistent with the 2017 EHT observations).

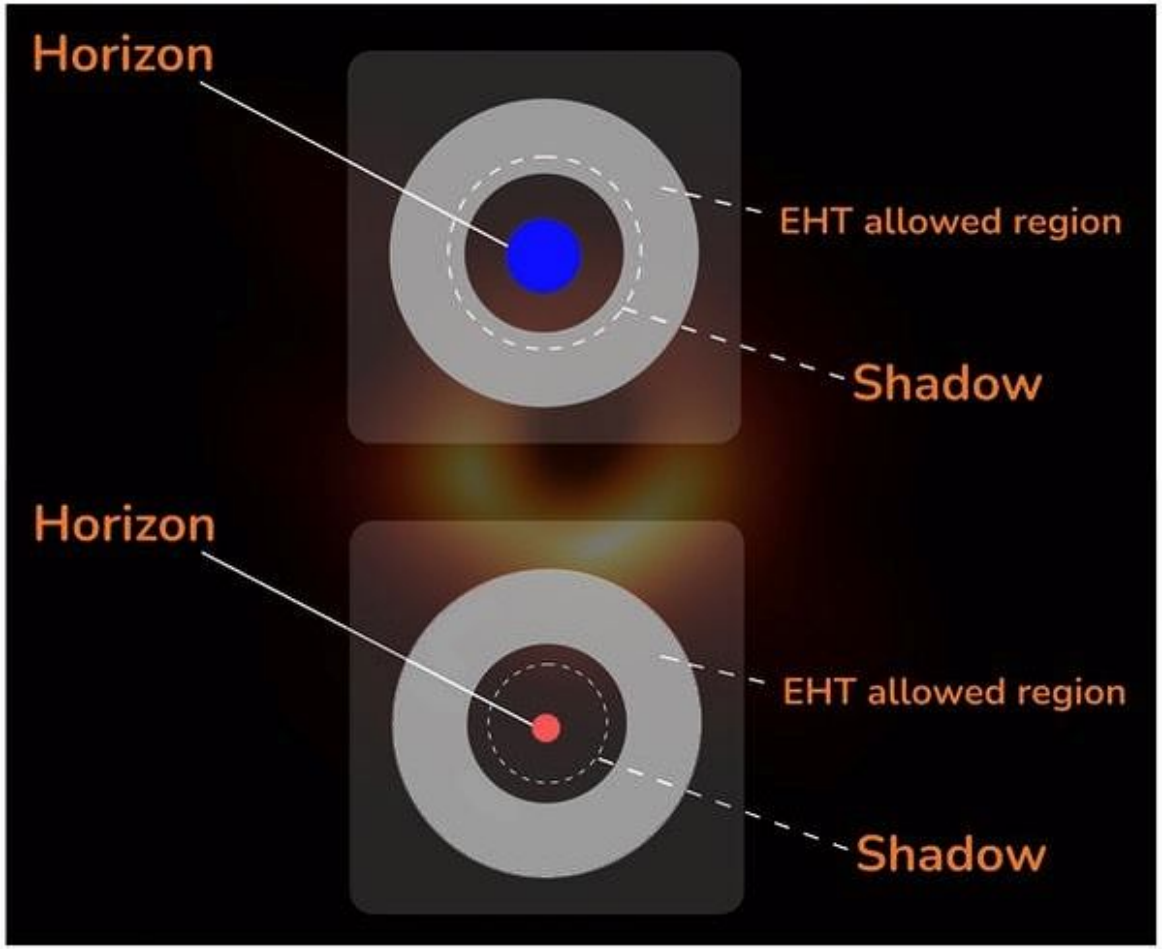
Horizon
EHT allowed region
Shadow
Horizon
EHT allowed region
Shadow

Zakharov, Universe, 2022; arxiv:2108.01533; charge constraint on M87* (for Sgr A* D=51.8±2.3 uas, 12.05.2022). For M87 D=D_Sch (1±0.17)

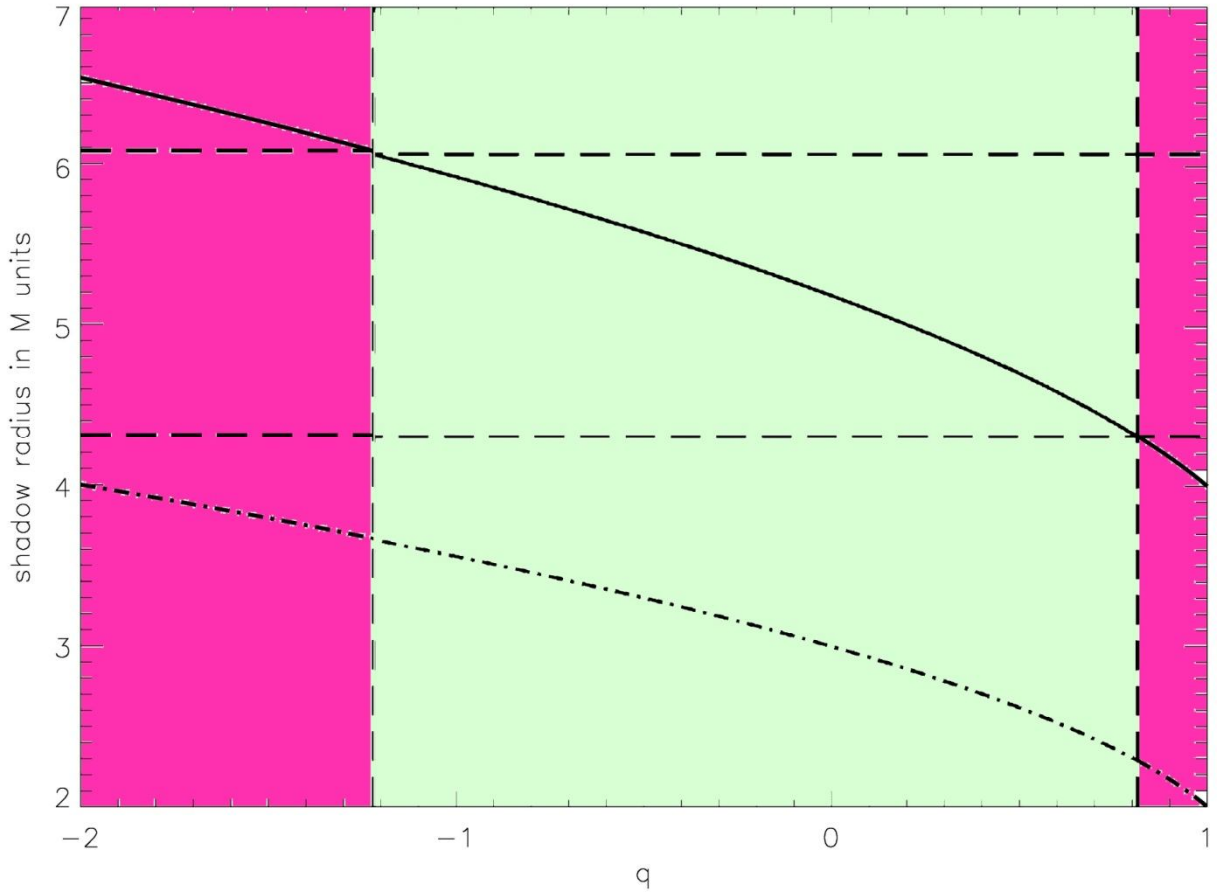

Sgr A* shadow discovery by EHT (reported on May 12, 2022)

Press Conferences around the world (Video Recordings):

Garching, Germany - European Southern Observatory

Madrid, Spain - Consejo Superior de Investigaciones Científicas

México D.F., Mexico - Consejo Nacional de Ciencia y Tecnología

Rome, Italy - Istituto Nazionale di Astrofisica

Santiago de Chile - ALMA Observatory

Washington D.C., USA - National Science Foundation

Tokyo, Japan - National Astronomical Observatory of Japan

For Sgr A* D=51.8±2.3 uas, (EHT collaboration, 12.05.2022)

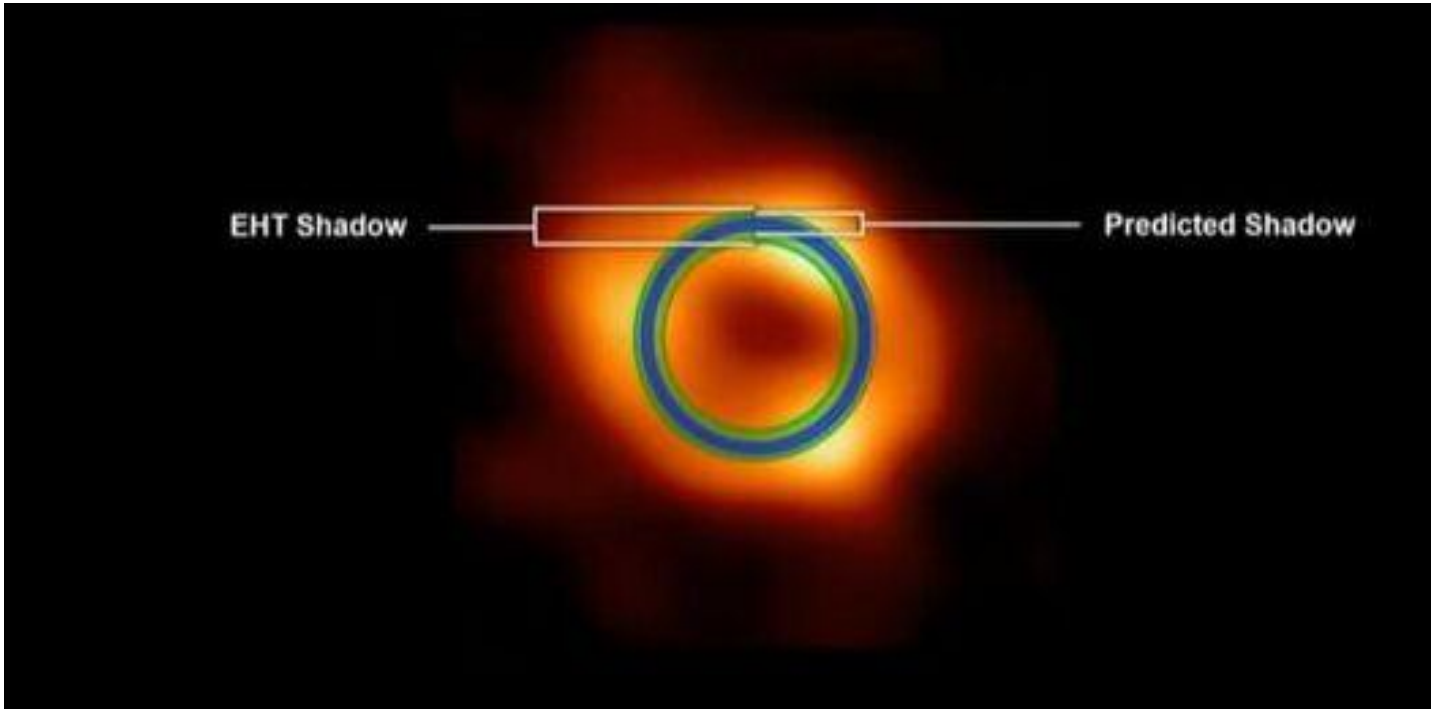

A. F. Zakharov, Physics of Particle and Nuclei Lett. (2023)

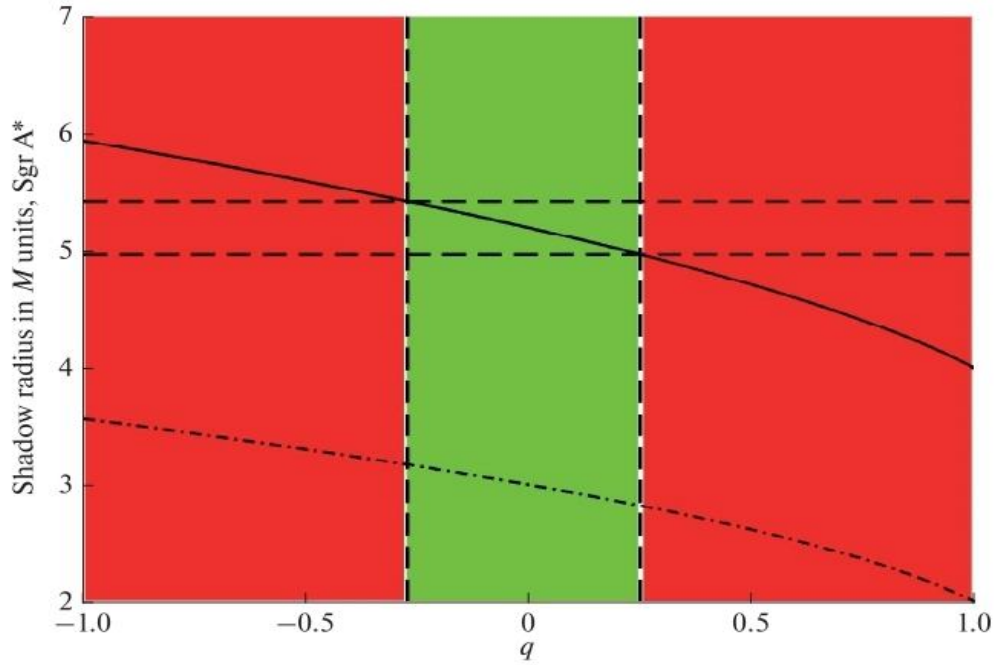

Fig. 1. Shadow radius (solid curve) and radius of the last circular unstable photon orbit (dashed-and-dotted curve) in units M as a function q. Following work [30], we believe that $\theta_{\text{sh SgrA*}} \approx (51.8 \pm 2.3)$ μas at a confidence level of 68%. The horizontal dashed lines correspond to the restrictions on the size of the radius in units M. Accordingly, red vertical stripes for q are inconsistent with these estimates of the size of the shadow in the HC.

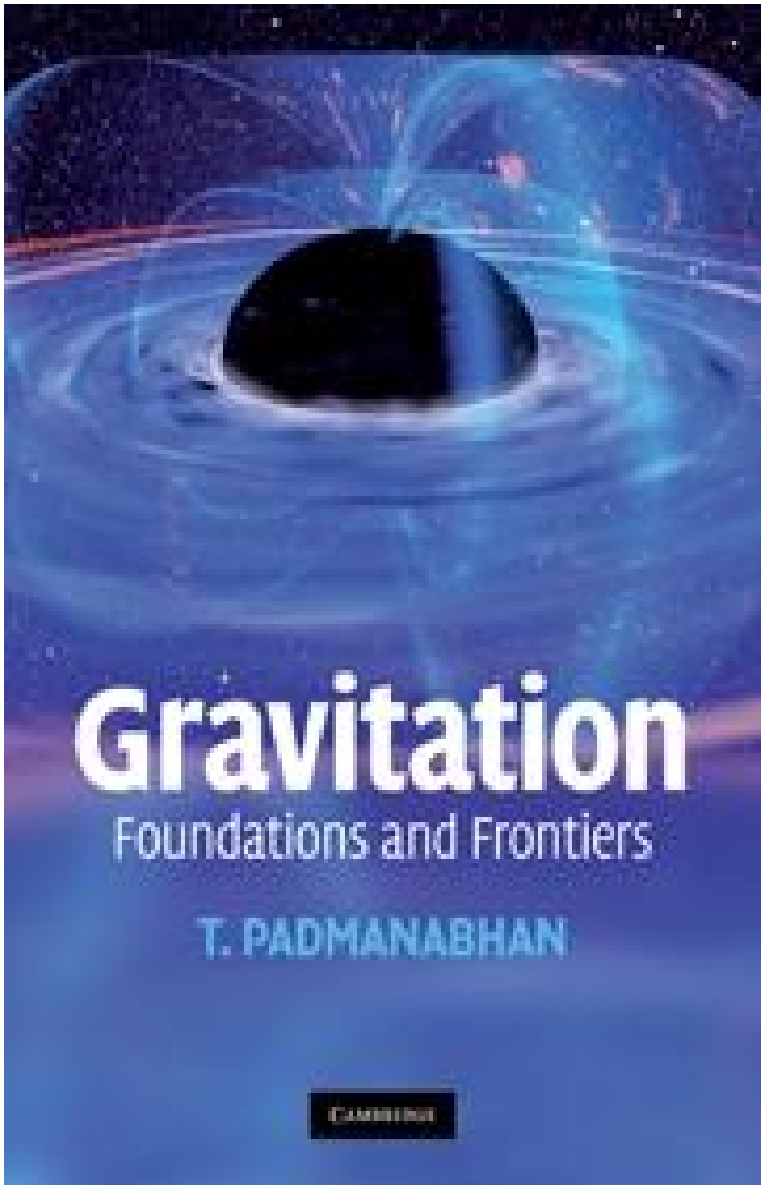
Gravitation
Foundations and Frontiers
T. PADMANABHAN
CAMBRIDGE

EXPLORING BLACK HOLES

Introduction to General Relativity

EDWIN F. TAYLOR
JOHN ARCHIBALD WHEELER
EDMUND BERTSCHINGER

SECOND EDITION

The Event Horizon Telescope Picture

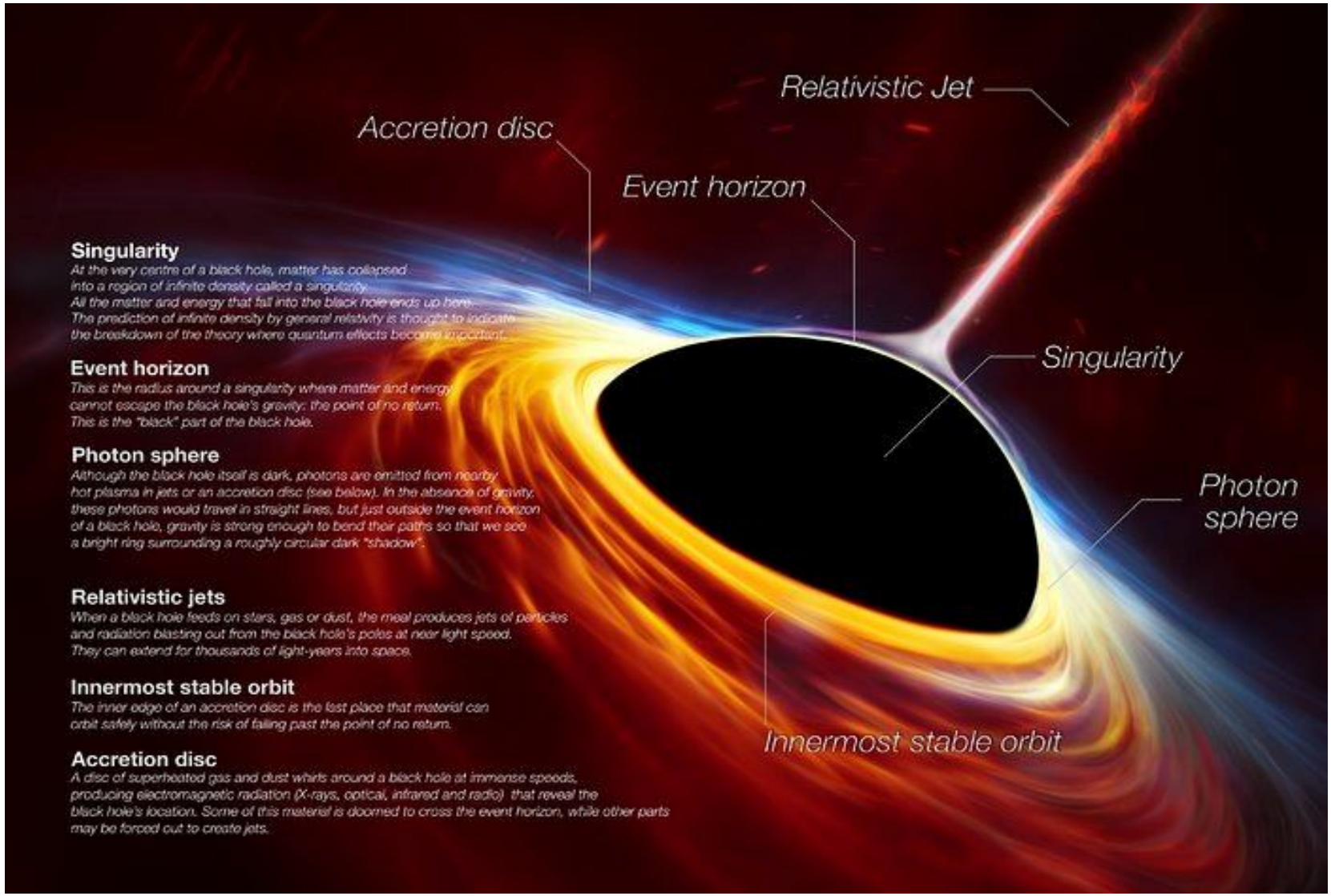

'A majestic story'
Financial Times

MICHIO KAKU

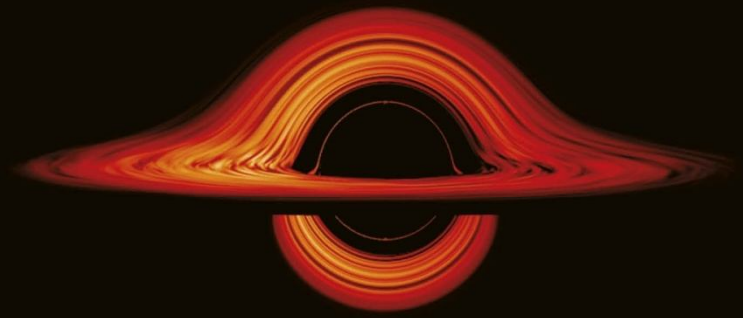

THE GOD EQUATION

The Quest for a Theory of Everything

Conclusion

The shadow concept has been transformed from a purely theoretical category into an observable quantity which may be reconstructed from astronomical observations.

Therefore, VLBI observations and image reconstructions for M87* and Sgr A* are in a remarkable agreement with an existence of supermassive black holes in centers of these galaxies.

Thanks for your kind attention!

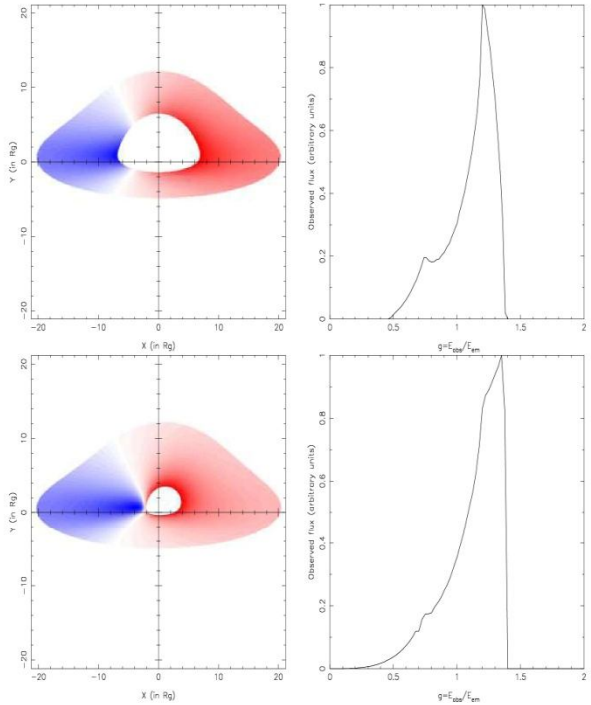

Fig. 2 (online colour at: www.fp-journal.org) The same as in Fig. 1 but for a highly inclined disk with $i = 75^\circ$.

asymmetric (see Fig. 3). If the line emission is originating at larger distances from the BH, the red peak of the line becomes brighter and line profile narrower and more symmetric. In majority of AGN, where the broad Fe Kα line is observed[1], its profile is more similar to the modeled profile as obtained under assumption that the line emitters are located close to the central BH. Therefore, comparisons between the observed and modeled Fe Kα line profiles can bring us some essential information about strong gravitational field in vicinity of central supermassive BH of AGN.

[1] Note here that in some AGN only the narrow Fe Kα line is observed, but it is supposed to be emitted in the disk corona that is located farther from the disk, and therefore, these relativistic effects cannot be detected in the line profile

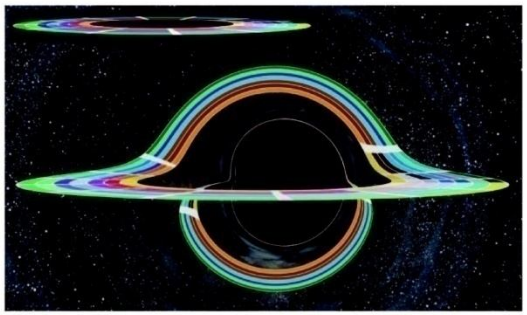

Figure 13. Inset: paint-swatch accretion disk with inner and outer radii $r = 9.26M$ and $r = 18.70M$ before being placed around a black hole. Body: this paint-swatch disk, now in the equatorial plane around a black hole with $a/M = 0.999$, as viewed by a camera at $r_c = 74.1M$ and $\theta_c = 1.511$ (86.56°), ignoring frequency shifts, associated colour and brightness changes, and lens flare. (Figure from *The Science of Interstellar* [40], used by permission of W. W. Norton & Company, Inc, and created by our Double Negative team, ™ & © Warner Bros. Entertainment Inc. (s15)).

itself. This entire image comes from light rays emitted by the disk's bottom face: the wide bottom portion of the image, from rays that originate behind the hole, and travel under the hole and back upward to the camera; the narrow top portion, from rays that originate on the disk's front underside and travel under the hole, upward on its back side, over its top, and down to the camera—making one full loop around the hole.

There is a third disk image whose bottom portion is barely visible near the shadow's edge. That third image consists of light emitted from the disk's top face, that travels around the hole once for the visible bottom part of the image, and one and a half times for the unresolved top part of the image.

In the remainder of this section 4 we deal with a moderately realistic accretion disk—but a disk created for *Interstellar* by Double Negative artists rather than created by solving astrophysical equations such as [32]. In appendix A.6 we give some details of how this and other Double Negative accretion disk images were created. This artists' *Interstellar* disk was chosen to be very anemic compared to the disks that astronomers see around black holes and that astrophysicists model—so the humans who travel near it will not get fried by x-rays and gamma-rays. It is physically thin and marginally optically thick and lies in the black hole's equatorial plane. It is not currently accreting onto the black hole, and it has cooled to a position-independent temperature $T = 4500$ K, at which it emits a black-body spectrum.

Figure 14 shows an image of this artists' disk, generated with a gravitational lensing geometry and computational procedure identical to those for our paint-swatch disk, figure 13

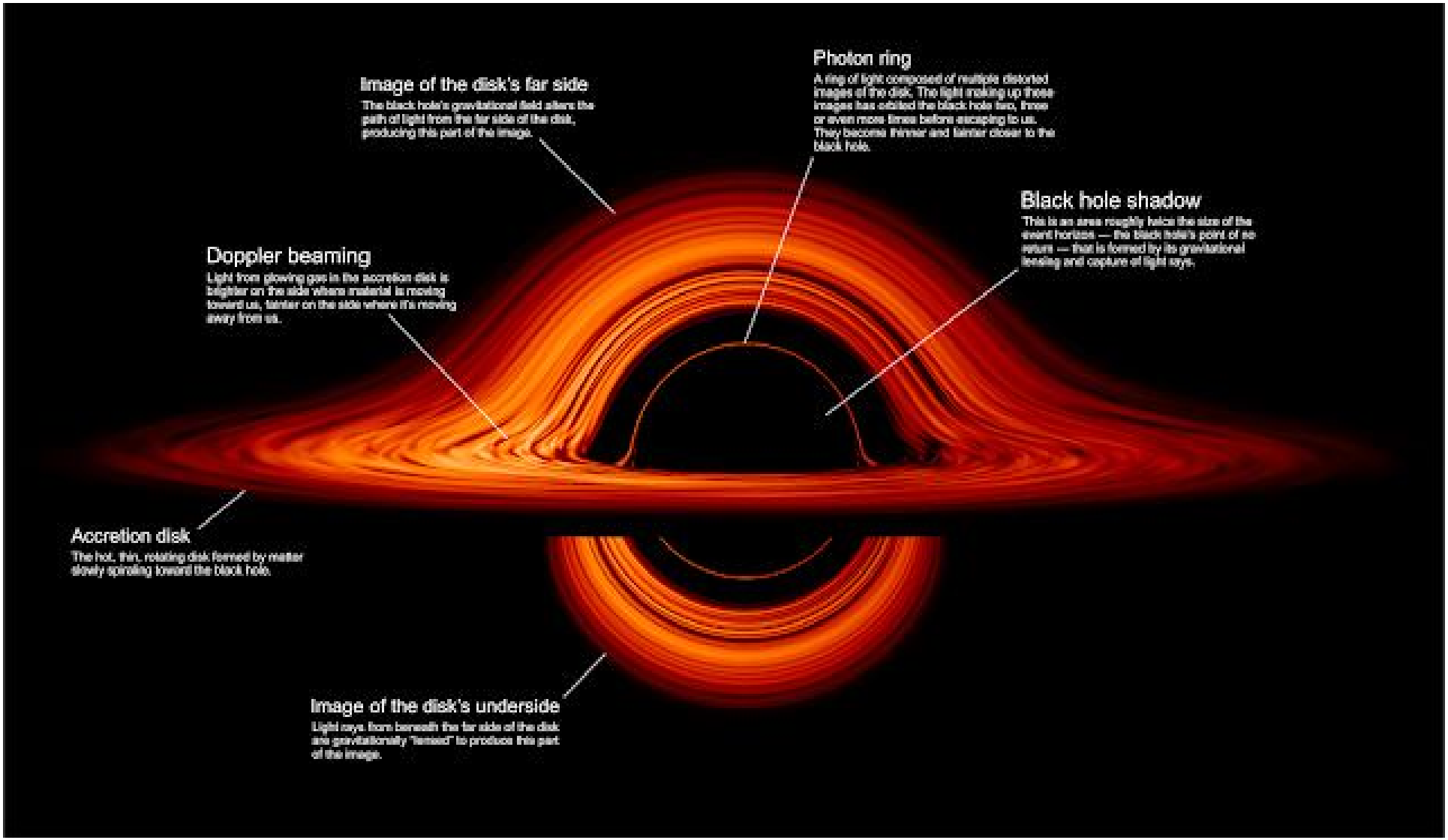
Image of the disk's far side
The black hole's gravitational field alters the path of light from the far side of the disk, producing this part of the image.
Photon ring
A ring of light composed of multiple distorted images of the disk. The light making up these images has orbited the black hole two, three or even more times before escaping to us. They become thinner and fainter closer to the black hole.
Black hole shadow
This is an area roughly twice the size of the event horizon — the black hole's point of no return — that is formed by its gravitational lensing and capture of light rays.
Doppler beaming
Light from glowing gas in the accretion disk is brighter on the side where material is moving toward us, fainter on the side where it's moving away from us.
Accretion disk
The hot, thin, rotating disk formed by matter slowly spiraling toward the black hole.
Image of the disk's underside
Light rays from beneath the far side of the disk are gravitationally "lensed" to produce this part of the image.

Fortschr. Phys. **56**, No. 4 – 5, 456 – 461 (2008) / **DOI** 10.1002/prop.200710519

Observational effects of strong gravity in vicinity of supermassive black holes

Predrag Jovanović[1,*] and **Luka Č. Popović**[1,2]

[1] Astronomical Observatory, Volgina 7, 11160 Belgrade, Serbia
[2] Alexander von Humboldt Fellow, presently at Max Planck Institute for Radioastronomy, Bonn, Germany

Received 27 November 2007, accepted 25 January 2008
Published online 8 April 2008

Key words Black holes, accretion and accretion disks, galactic nuclei, active and peculiar galaxies and related systems, quasars

PACS 97.60.Lf, 97.10.Gz, 98.62.Js, 98.54.Cm, 98.54.-h

Here we discuss the effects of strong gravity that can be observed in electromagnetic spectra of active galactic nuclei (AGN). According to the unification model of an AGN, there is a supermassive black hole ($10^7 - 10^9 M_\odot$) in its center, surrounded by an accretion disk that radiates in the X-ray band. Accretion disks could have different forms, dimensions, and emission, depending on the type of central black hole (BH), whether it is rotating (Kerr metric) or nonrotating (Schwarzschild metric). We modeled the emission of an accretion disk around supermassive BH using numerical simulations based on a ray-tracing method in the Kerr metric. A broad emission line Fe Kα at 6.4 keV with asymmetric profile (narrow bright blue peak and a wide faint red wing) has been observed in a number of type 1 AGN. The effects of strong gravitational field are investigated by comparison between the modeled and observed iron Kα line profiles. The results of our modeling show that the parameters of the Fe Kα line emitting region have significant influence on the line profile and thus, allow us to determine the space-time geometry (metric) in vicinity of the central BH of AGN, and also can give us information about the plasma conditions in these regions.

1 Introduction

It is now widely accepted that AGN derive their extraordinary luminosities (sometimes more than 10^4 times higher than luminosities of "ordinary" galaxies) from energy release by matter accreting towards, and falling into, a central supermassive BH. The accretion disks around the central BH represent an efficient mechanism for extracting gravitational potential energy and converting it into radiation, giving us the most probable explanation for the main characteristics of AGN (high luminosity, compactness, jet formation, rapid time variation in radiation and the profile of the Fe Kα spectral line). Thus, AGN are powerful sources of radiation in a wide spectral range: from γ rays to radio waves [1].

The most important feature of the X-ray radiation of AGN (which is generated in the innermost region around a central BH) is a broad emission line Fe Kα at 6.4 keV that may have an asymmetric profile (narrow bright blue peak and wide faint red peak). It was discovered in Seyfert 1 galaxy MCG-6-30-15 [2] and later on observed in a number of AGN. In some cases the line width corresponds to one third of speed of light, indicating that its emitters rotate with relativistic velocities. Therefore, the line is probably produced in a very compact region near the central BH of AGN and can provide us some essential information about the plasma conditions and the space-time geometry in vicinity of the BH [3].

* Corresponding author E-mail: pjovanovic@aob.bg.ac.yu, Phone: +381 11 3089 068, Fax: +381 11 2419 553